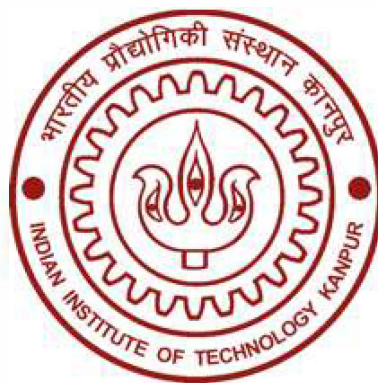


ESO 205

Nature and Properties of Materials

Laboratory Manual



Department of Materials Science and Engineering

**Indian Institute of Technology
Kanpur
2018-19**

EXPERIMENT 1

Objectives:

The objectives of this experiment are to visualize various structural characteristics of a crystal structure, and get familiarized with X-ray diffraction, an important technique used for determining the crystal structure.

Specifically, after completion of this experiment a student is expected to

- Know the difference between a Crystal - Lattice and Crystal – Structure.
- Create simple crystal structures (monatomic decoration of FCC and BCC lattices).
- View the various physical characteristics of a crystal structure such as planes, voids, etc., as well as crystallographic-directions from different orientations, and develop a visual feel for these.
- Measure the distance between atoms, angles between directions/planes.
- Generate X-ray diffraction pattern using the software for a given crystal-structure. Extract some preliminary information about a crystal structure from its X-ray pattern.

This experiment has been divided in two parts:

- A) Visualization of crystal-structures and related features using CaRIne crystallography software.
- B) Using X-ray diffraction pattern to determine crystal-structure.

PART A

Visualization of crystal-structures and related features using CaRIne crystallography software

Before we learn about the software, let's familiarize ourselves with some basic definitions/information regarding crystals lattice/structure:

1. **Crystal-Systems:** The 3-dimensional space can be divided into smaller volume units such that each unit is made of three sets of planes. When one thinks of all such possible volume units that can be repeated onto each other while maintaining the same orientation as the starting unit volume, there are only seven such unit volumes that will span the entire space without leaving any gap between them. These 7 unit volumes are known as **7 crystal-systems**. That are: (1) Triclinic, (2) Monoclinic, (3) Orthorhombic, (4) Tetragonal, (5) Cubic, (6) Rhombohedral, and (7) Hexagonal. A crystal-system is identified by the lengths of the 3 sides (viz. a , b , c) of the unit volume-space and the 3 angles (α , β , γ) between these three sides.

Note: For each of the above mentioned unit-cells there are 6 faces.

But it is possible to divide 3-D into such volume-units where each unit is surrounded by more than 6 faces, and these units when placed onto each other while maintaining the relative orientation can span the entire space without leaving any gap between them.

2. **Crystal-Lattice:** A *crystal-lattice* is defined as a periodical arrangement of geometrical-points in 3-dimensional space in such a way that each point has identical environment around it. By identical environment it is meant that when the lattice is observed from different lattice-points (one point at a time) in a particular orientation, it looks identical from each of the points. A lattice is a mathematical concept; there are no atoms or molecules located at these points
3. **Bravais-Lattice:** When one looks for all the possible arrangements of geometrical-points in the above mentioned seven crystal-systems such that these points conform to the translation and orientation constraints of a Crystal-lattice, one finds there are total 14 such arrangements of points in 3-D. The special arrangements are identified as **14 Bravais Lattices**.
4. **Primitive unit-cell & Conventional unit-cell:** The primitive-unit cell is the smallest volume which contains exactly one lattice point, and when it is translated by all the vectors in a Bravais-lattice (vectors connecting a lattice-point, selected as an origin, to all other lattice-points).

A conventional unit-cell is larger than primitive unit-cell containing more than one lattice points. It also satisfies the criteria of a unit-cell i.e. when it is translated by some sub-set of Bravais-lattice vectors, it spans the entire lattice. Generally the conventional unit-cells are used because they easily reveal the geometrical-symmetry of the lattice.

5. **Basis/Motif:** The basis/motif is the minimal unit which when placed at lattice points, gives rise to a physical crystal. The basis can be an atom, a molecule, an ion etc.

6. **Crystal-Structure:** A crystal-structure is a regular arrangement of a physical unit called basis/motif at all the points of a Bravais-Lattice.

Note, that when the basis/motif consists of single atomic unit, the resulting crystal-structures are said to be belonging to Bravais-lattice. This is because, when such a crystal-structure is observed from any atom it is made of, while maintaining the same viewing orientation every time, the crystal-structure looks identical. This condition also requires that each **single atom must belong to the same element**.

On the other hand, in general, when the basis/motif consists more than one atom; the resulting crystal-structure usually doesn't retain the characteristics of having-identical-view from-all-the-individual-atoms. And therefore, such crystal-structures are identified as non-Bravais lattice. Sometime these are also identified as lattice with a basis.

7. **Crystallographic-planes and Miller Indices:** Due to periodic arrangement of motifs/basis they can be visualized as if lying in a plane, and these are identified as crystallographic-planes.

Usually Miller indices are used to indicate the planes. If a plane intercepts the three axis at a_1a , a_2b and a_3c distance from the origin, where a , b , and c are lattice parameters along the three axis. The corresponding Miller indices are calculated by:

- 1) Taking the reciprocal of the three numbers: a/a_1a , b/a_2b , c/a_3c , which results into ratios: $1/a_1$, $1/a_2$, $1/a_3$
- 2) Finding the lowest common multiplier (LCM) for the obtained fractions such that multiplication of it with the three ratios gives a set of 3 integrals numbers.

For example a plane intersecting the axes at $2a$, $5b$, $2c$ will have Miller indices of $5,6,5$. The Miller Indices of a plane are shown in parentheses without any comma separator. Therefore for the current plane the Miller indices are (565) . These indices also represent all the other planes that are parallel to the plane for which we have calculated these indices.

8. **Crystallographic direction:** A direction in a crystal having the form of $ua + vb + wc$ is said to have a crystallographic direction as $[uvw]$. It also represents all the other vectors that are parallel to the given vector. Here **a**, **b**, and **c** are vectors along the three crystal axis.

9. **Voids:** The vacant space between the atoms in a crystal structure is identified as interstitial voids. Two types of voids are, 1) Tetrahedral and 2) Octahedral void.

CARINE CRYSTALLOGRAPHIC SOFTWARE

Following instructions about using the software help visualize different features of a crystal within the limitations of the present version.

Note: All word in between the following sentences that are **Bold**, represent a tool option available in CaRIne, unless mentioned otherwise.

1.0 Accessing the software:

This software has been installed on selected computer in the laboratory. To open this software double-click on the desktop icon titled *CaRIne 3.1*. Do not select *CaRIne 3.1-sr*, it has very limited capabilities. A window will open similar to that shown in figure. 1.

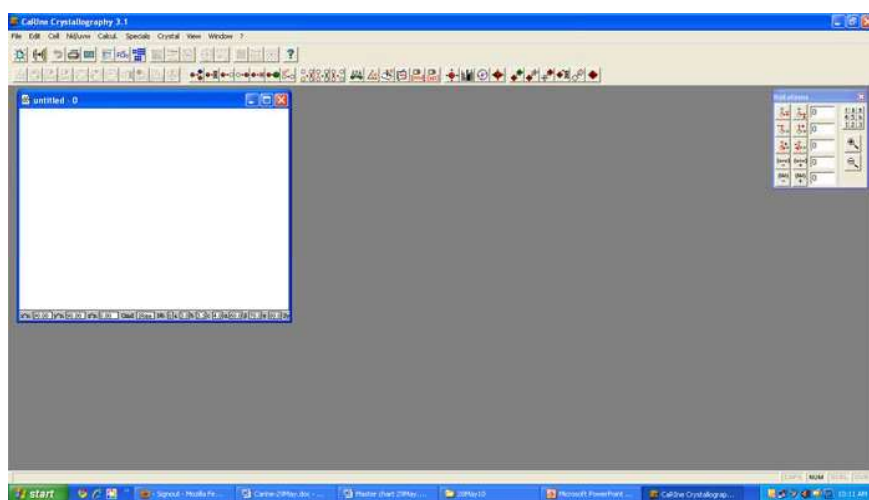


Figure 1: The main window of the CaRIne software showing crystal structure window.

1.1 Drawing a crystal structure

Go to **Cell** menu, and select one of the crystal systems from the drop-down menu. Figure 2 shows a unit cell of Face-centered-cubic (FCC) unit-cell.

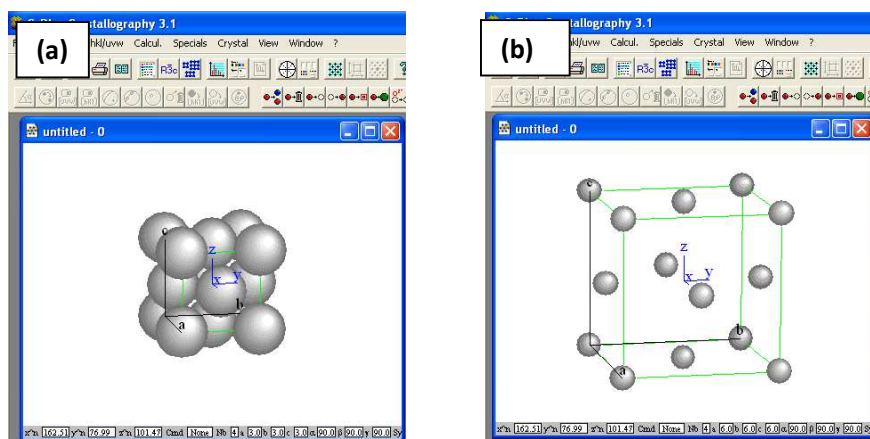
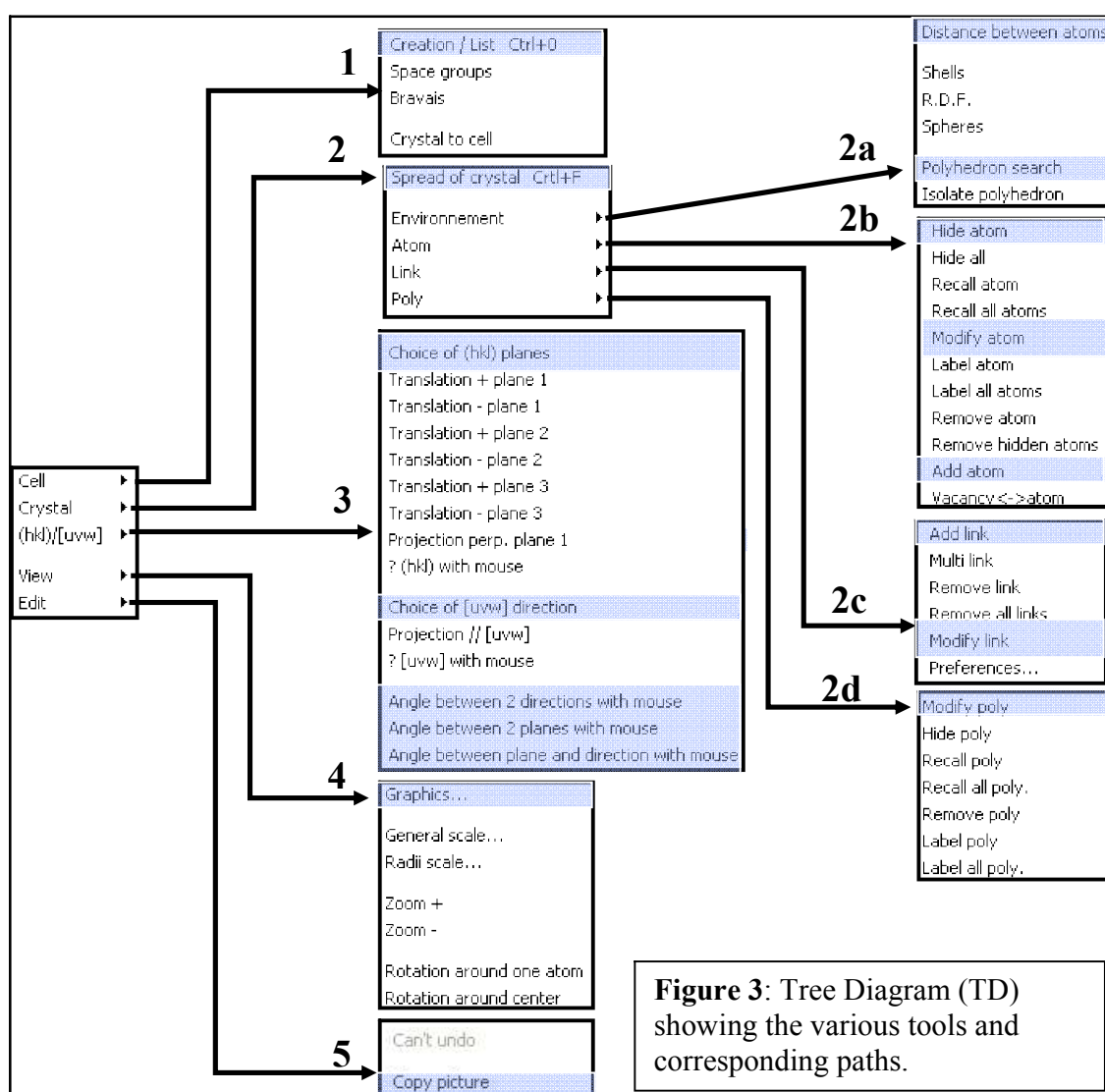


Figure 2: An FCC unit cell (a) without and (b) with modifications.

- Viewing the structure from different directions: A crystal structure can be viewed from different orientations by holding the *Ctrl* key pressed and using the left button of the mouse to change the orientation.

Like changing the viewing direction as mentioned above, there are several other tools available to visualize/modify the crystal model in different ways. To access these tool right-click while being in the crystal structure window; a menu be displayed. This menu along and its different sub-menus have been shown in the form of a tree-diagram (TD) in figure 3.

For the instructions that follow, the term **path** will always refer to the tree-diagram unless mentioned otherwise.



Let's see what is available for path 1 in this Tree Diagram. By following path 1 and selecting **Cell Creation/Cell List** a window will open as shown in figure 4. Utilities in this window will be used most of the time during visualizing a crystal structure, and they have been indicated in the figure itself.

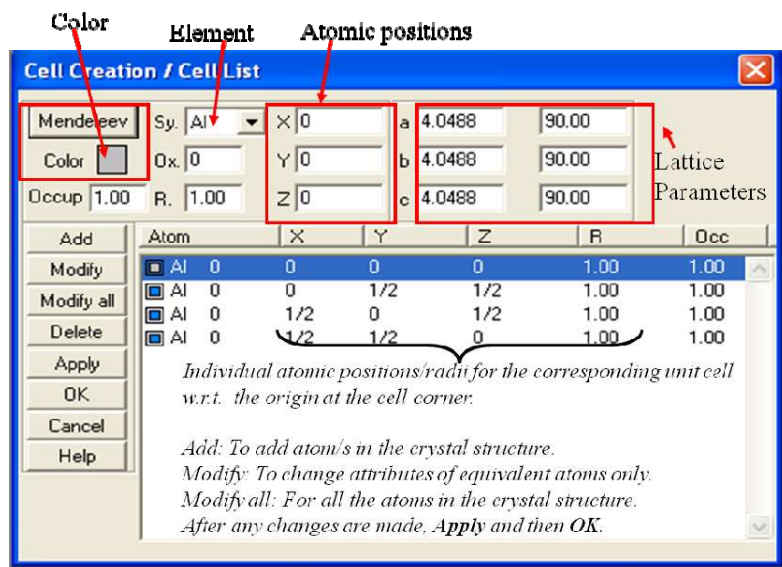


Figure 4: Cell Creation/Cell List window showing various attributes that can be modified for better visualization.

1.2 Visualizing planes and directions

1.2.1 Planes:

After selecting the crystal-window for which a plane has to be visualized, follow path 3 and select **Choice of (hkl) planes**; a new window will open where (hkl) values for up to three different planes can be entered.

For example, if (111) plane for FCC crystal structure is to be visualized, after accessing **Choice of (hkl) planes**, enter $h = 1$, $k = 1$, and $l = 1$ and hit OK. It will highlight the atoms lying on the plane as shown in the figure 6.

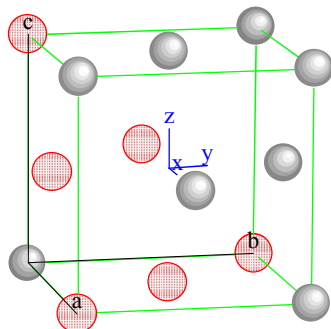


Figure 5: Red colored atoms showing (111) plane in a FCC unit cell.

Let us learn about few more tools that help visualize the planes in different ways.

- Spread of crystal: With this tool one can extend the crystal structure by desired number of unit cells along any one or all the three directions. It can be assessed by path 2.

For example, if (111) plane is visualized while using this tool it will look like as shown in figure 6(a) after translating the plane, as explained below.

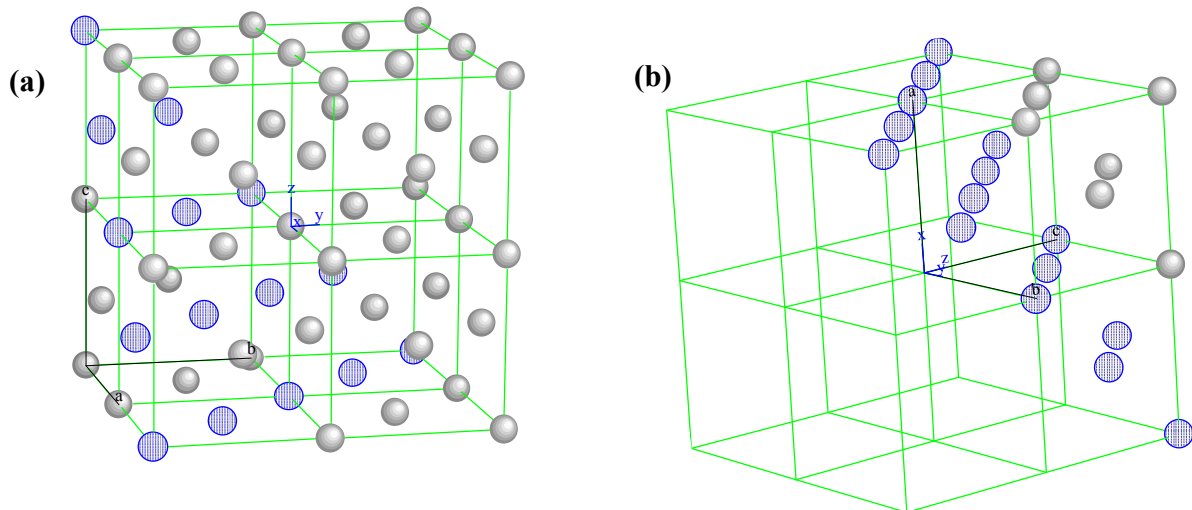


Figure 6: (a) Atoms in (111) plane after spreading the FCC unit cell, (b) Similar plane with the atoms removed using the **Cut** option.

- Changing color of the atoms lying in one plane: Once a plane has been identified as explained above, double-click on any atom in the plane. A new window will open where color attributes can be changed.

The Following tools are meaningful only when the crystal has been expanded using **Spread of crystal**.

- Translation of the plane: A plane can be translated by one interplanar spacing at a time by selecting the option **Translation + plane 1** which can be assessed by following path 3.
- Cut: This helps to visualize a plane in a similar way as shown in figure 6(b). For this, follow path 2 and select **Spread of crystal**. In the window that opens enable the **Center** option. This brings the origin point of the crystal unit-cell and origin of the X-Y-Z coordinate together. Now, follow path 3 → select **Choice of (hkl) plane** → enable **Cut** option. The will result into a crystal that will look similar to what is shown in figure 6(b).

- Viewing the crystal along perpendicular to the plane: Follow path 3 and select **Projection perpendicular plane 1.**

1.2.2 Directions:

There are two ways by which a crystallographic direction ($\mathbf{R} = u\mathbf{a} + v\mathbf{b} + w\mathbf{c}$) can be visualized:

- By providing values for u, v, w (integral values):
 ➔ Follow path 3 and select **Choice of [uvw] direction.**
- By selecting any two atoms with computer mouse along the desired direction
 ➔ Follow path 3 and select **?[uvw] with mouse.**

Note: The limitation of this software is that when the direction is visualized within a single unit cell, the direction doesn't start from the origin linked to the unit cell (fig. 7a). This limitation can be overcome with the help of following trick:

For path 2 select **Spread of Crystal**, add 2 unit cells in all the three directions and select **Build from Center** option. Now any specified [uvw] direction will start from the origin attached to the unit cell as shown in figure 7(b).

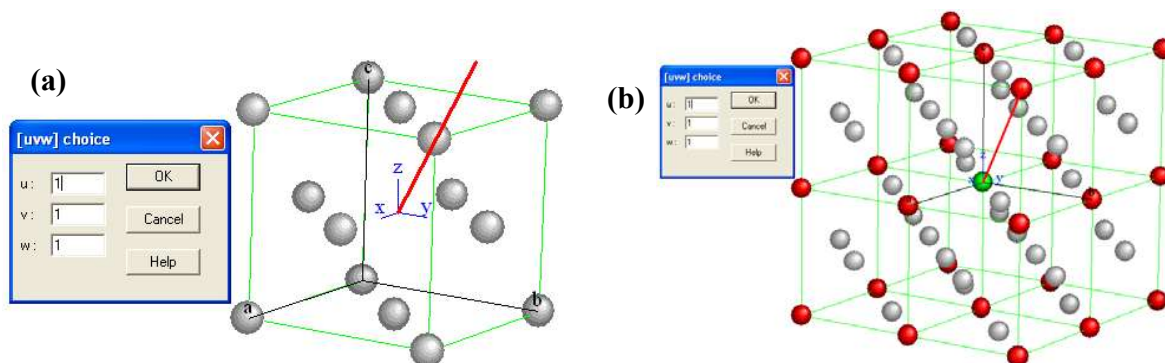


Figure 7: (a) Direction drawn in single unit cell, (b) Direction drawn after spreading the crystal.

1.3 Distance between atoms, and angles between directions/planes in a crystal structure.

- **Distance between atoms:** Follow path 2a and select **Distance between atoms.** Now select two desired atoms (by mouse) and a pop-up window (fig. 8a) will display the distance.
- **Angles between directions / planes:** Follow path 3 and select the appropriate option out of the three options at the bottom of the sub-menu, whichever is. For example, figure 8(b) shows the angles between two planes.

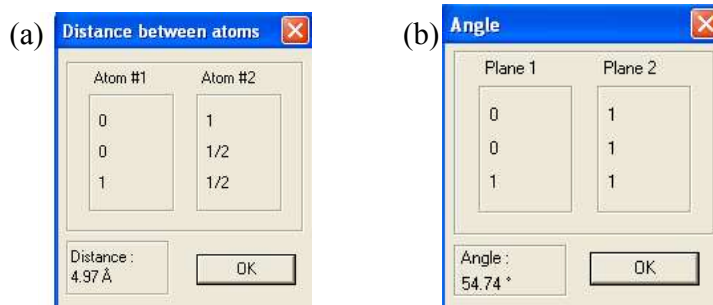


Figure 8: (a) Showing atomic positions and the corresponding distance between two selected atoms, and (b) (hkl) indices of the two planes and the corresponding angle are shown.

1.4 To visualize a void in a crystal structure:

Following stepwise procedure shows how to visualize an octahedral void in FCC crystal structure. Similar approach is applicable for other types of voids.

Approach #1:

- 1) Create a FCC unit cell
- 2) Follow path 1 and select **Creation/List** option. Here, you may change the lattice parameter/radii/color etc. to get a better visualization of the crystal structure. For example, as shown in figure 9 corner and face-centered atoms are colored differently, or as shown in figure 10, the corner atoms have been removed, for better visualization.

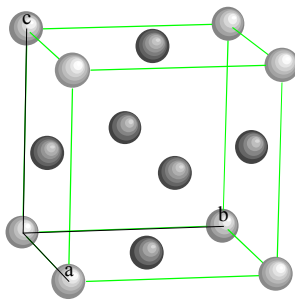


Figure 9: A FCC unit cell with atoms at equivalent positions colored differently.

- 4) Follow path 2c and use **Link** option to connect desired atoms. Link allows only two atoms to be connected at a time; the **multi-link** option results into computer hang. Save the file before you try **multi-link** option.

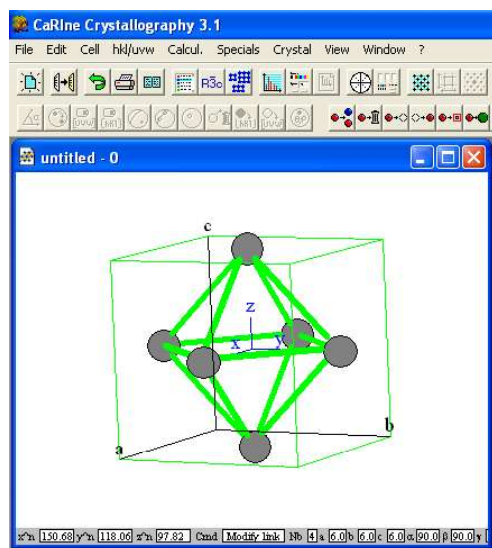


Figure 10: An octahedral void with removed corner atoms.

Approach #2:

Note: This option works only when you there is a dummy atom at the center of the void to be visualized. This dummy atom can be kept very small in size so that it can be recognized as a dummy atom.

- 1) Path 1 → **Creation List**, and use **Add atom** to incorporate an extra atom at the centre of the octahedral void i.e. at position co-ordinates (1/2, 1/2, 1/2). In figure 11, this atom has been given blue color.

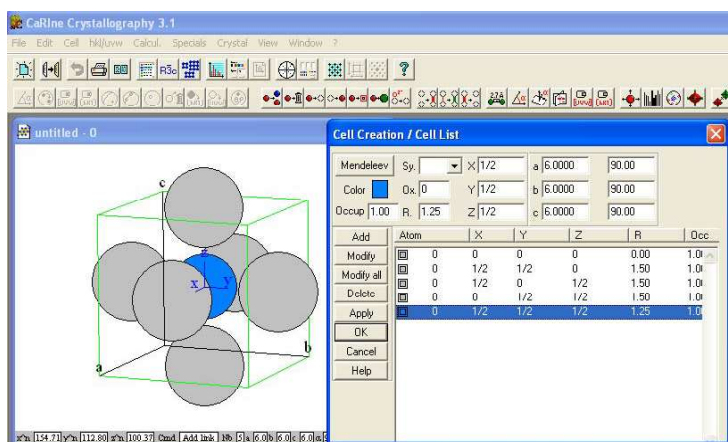


Figure 11: A dummy atom at the center of an octahedral void. It has been given blue color to identify it separately. Also the corner atoms have been removed for better visualization.

- 2) Now we have to make a polyhedron connecting the atoms forming octahedral void. For this, follow path 2a and select the **Polyhedron search** option.

- 3) Click on the dummy atom. Another window will open, as shown in figure 12, where a list of atoms will be present. To explain a little about this list, the top-most entry in this list shows the first set of nearest neighbors for the dummy atom along with total number of such atoms and their distance from the dummy atom. The second entry shows the number of second nearest atoms and their distance from the dummy atom, and so on.

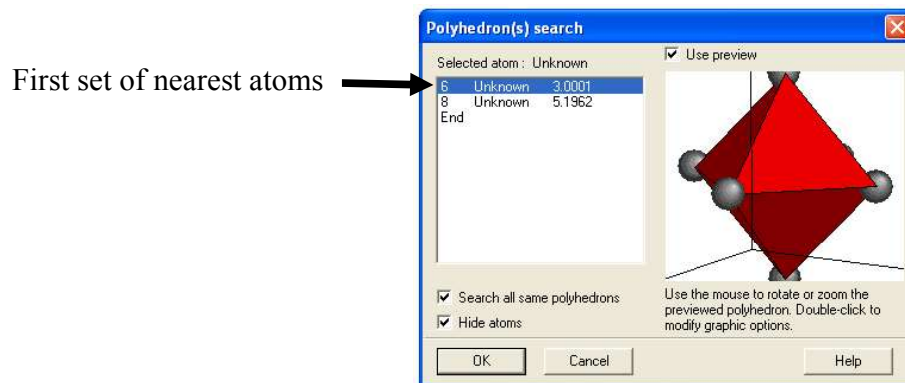


Figure 12: The red polyhedron is formed by the set of 6 nearest atoms around the octahedral void.

- 4) Since in the present case, the void (dummy atom) is surrounded by 6 nearest atoms, we select the first entry in the window. Also enable *Use Preview*, it will show how the polyhedron will look like. By hitting *OK*, the polyhedron will be made on the crystal under consideration, and it will look similar to that in figure 13.

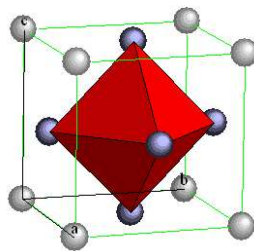


Figure 13: An octahedral polyhedron formed by 6 face-centered atoms in a FCC structure.

- 4) To get an array of octahedral polyhedrons as shown in figure 14, for the FCC unit cell where we just drew the polyhedron (fig. 13), use **Spread of Crystal**. After spreading the unit cell the polyhedron may disappear, and therefore the polyhedron has to be redrawn on the stretched crystal structure by following the steps 3) & 4).

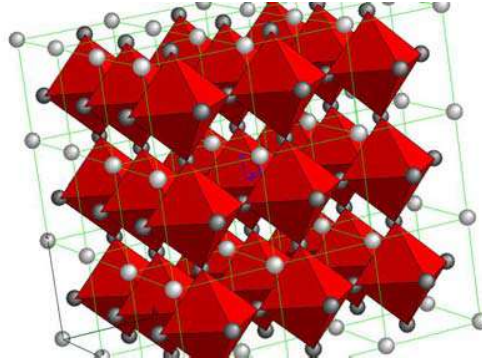


Figure 14: An array of octahedral polyhedrons in FCC structures.

This ends the instructions for **Part A**. Next, instructions for part B have been given.

PART B

X-ray diffraction pattern to determine crystal-structure

1) Introduction:

X-ray diffraction (XRD) is an important characterization technique for obtaining the information about crystal structure of a given material, identify the elements/phases by comparison with the database of XRD pattern for known materials, find out surface-orientation in case of a single crystal, and quantify the cell parameters, crystallite size as well as other structural parameters.

2) Working principle in brief:

X-rays are electromagnetic waves with wavelength in the range of $100 - 0.1 \text{ \AA}$ ($10 - 0.01 \text{ nm}$); the X-ray wavelength used for XRD technique is of the order of few angstroms, e.g. generally used X-ray is $\text{Cu K}_\alpha = 1.54 \text{ \AA}$. For comparison, the wavelength of the visible electromagnetic spectrum lies between $4000 - 7000 \text{ \AA}$ ($400 - 700 \text{ nm}$). If we compare the magnitude of these wavelengths with the typical value of inter-atomic distance in a material which is in the range of few Angstroms (for Copper it is 2.55 \AA), it is clear that the wavelengths for visible spectrum are thousands of times longer compared to the inter-atomic distance, while that used for XRD are comparable to the inter-atomic distance. This is why the X-rays experience the discreteness of the material, and are diffracted by the constituent atoms. These diffracted X-rays from the atoms interfere with each other constructively or destructively depending on their phase difference, and it leads to the observation of intense diffraction peaks for particular incident directions (angles). These strong diffraction peaks reveal the family of parallel sets of planes that diffracted the X-ray present in the crystalline material, and this information in-turn, can be used to unlock the information about the crystal-structure of that material. When this observation of constructive and destructive interference is put together in a mathematical form, a simplified version of it is given by the following expression (Eq.1), known as Bragg's Law, named after W. L. Bragg and W. H. Bragg who first proposed it. This expression can be pictorially shown in figure. 1.

$$N \lambda = 2 d_{hkl} \sin\theta \quad (1)$$

In this expression for Bragg's law:

- λ is the wavelength of incident monochromatic X-rays,
- d_{hkl} is interplanar distance (distance between the two consecutive planes) from the set of parallel planes having miller indices (hkl),
- θ is incident angle (angle between the X-ray beam and the surface), and
- N (an integer) is order of the diffracted beam.

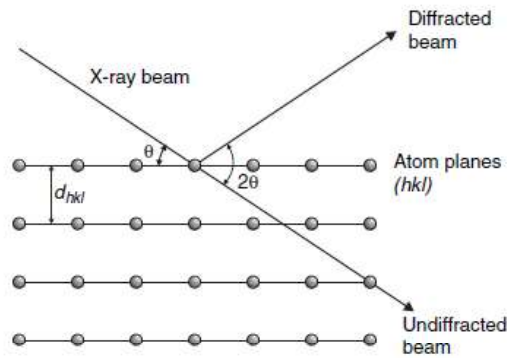


Figure 1. Diffraction of X-rays from a set of (hkl) plane [1].

A typical XRD pattern generated using CaRIne Crystallography software for a simple cubic structure having lattice parameter 3 Å (an arbitrary value which is very close to typical lattice parameter for real elemental materials) is shown in figure. 2.

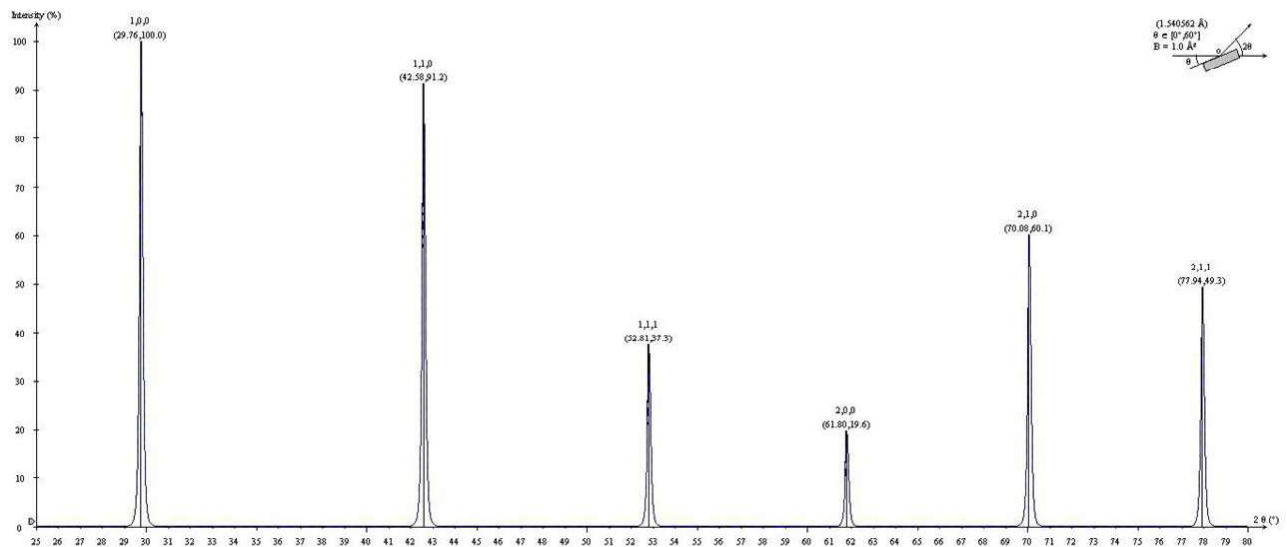


Figure 2. XRD pattern for the simple cubic crystal lattice

In figure 2 the y-axis is intensity of the diffracted peaks. For X-axis you might have noticed that the angle is 2θ and not θ . This is because, as shown in figure.1, for the X-ray beam incident at an angle θ the angle between the incident and diffracted **direction** is 2θ . To put it in other words, in practice the X-ray source is kept stationary and the sample is rotated, and for a rotation of the sample by θ the detector has to be moved by 2θ .

3) Other information which can be obtained from a XRD pattern:

- **Estimation of grain size from peak width:**

The peak width $\partial\theta$ (in radians), measured at half the height of the intensity-peak, also known as full-width-at-half-maximum (FWHM), is inversely proportional to the crystallite size D_{hkl} . The mathematical equation correlating the two parameters is given as [1]:

$$\partial\theta \approx \frac{\lambda}{D_{hkl} \cos \theta} \quad (2)$$

Here, $\partial\theta$ is peak width in radians at FWHM, λ is wavelength of the incident X-ray, D_{hkl} is crystallite-size in the direction normal to the (hkl) plane, θ is the Bragg angle for the peak under consideration. You will notice that this equation is sometimes also identified by the name of Scherrer Equation, in the literature. This equation (Eq. 2) is valid only when the crystallite size is less than 100 nm. Also, note that this equation gives only rough estimates about the crystallite size; a much better technique is electron microscope to measure the crystallite size.

- **Selection Rule:**

Depending on the specific arrangement of atoms in a unit cell, for some of the (hkl) planes where we expect strong peaks, there are no peaks!, they are systematically absent from the XRD pattern. The correlation between the arrangement of atoms in a unit cell and the absence of particular (hkl) intensity peaks leads to *selection-rules*. Following table shows the selection rule for a cubic crystal lattice i.e. for simple cubic, BCC and FCC Crystals. The information on missing peaks can be used to get an idea about crystal-lattice for a material from its XRD pattern.

Lattice	Reflection present	Reflection absent
Simple Cubic	For all h, k, l values	None
Body-Centered Cubic (BCC)	For $h+k+l = \text{even number}$	For $h+k+l = \text{odd number}$
Face-Centered Cubic (FCC)	For h, k and l either all even or all odd	For h, k, l values mixed, i.e. some are even while remaining are odd

For details of the selection rule, you may refer to Ref. 1 and 2.

- **Lattice parameter:**

By noticing the 2θ position of a (hkl) peak the interplanar distance d_{hkl} can be calculated using Eqn. 1. The correlation between the interplanar distance d_{hkl} for a (hkl) plane and the lattice parameters a, b, c is [1]:

$$\frac{1}{d_{hkl}^2} = \sqrt{\left(\frac{h}{a}\right)^2 + \left(\frac{k}{b}\right)^2 + \left(\frac{l}{c}\right)^2} \quad (\text{Only when } \alpha = \beta = \gamma = 90^\circ) \quad (3)$$

USING CARINE CRYSTALLOGRAPHY SOFTWARE TO GENERATE X-RAY DIFFRACTION PATTERN:

Note: All word in the following sentences that are **Bold**, represent a tool option available in CaRine.

- Following is a stepwise procedure that allows one to generate a XRD pattern for selected a crystal structure:

Step #1: Selecting the crystal system

- On the software window, click the icon **Cell** and from the drop-down menu select the desired crystal structure. Complete the process so that you see a model of the crystal on the screen as shown below in figure 3.

Step #2: Generating the corresponding X-ray diffraction pattern

- Click the icon **Special**, and from the drop down menu select **XRD** followed by **Creation XRD**, as shown below in figure. 3.
- Once you select **Creation XRD**, another window, as shown in figure. 4 will open. In this window the wavelength of the incident monochromatic X-ray, and Bragg angle range has to be specified. Here the angle entered is regarded as θ and not 2θ , i.e. if you select angle range $10 - 60^\circ$, the generated XRD pattern will be shown for the angle range $20 - 120^\circ$.

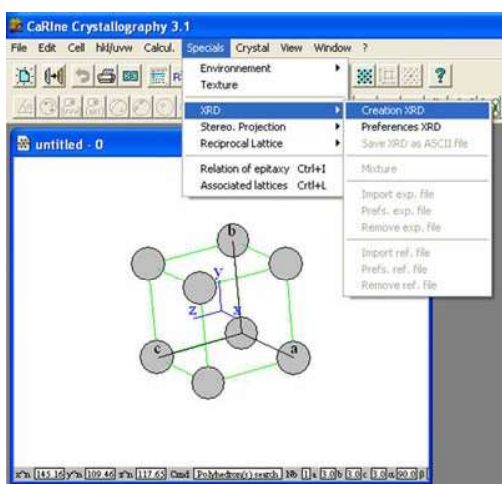


Figure. 3

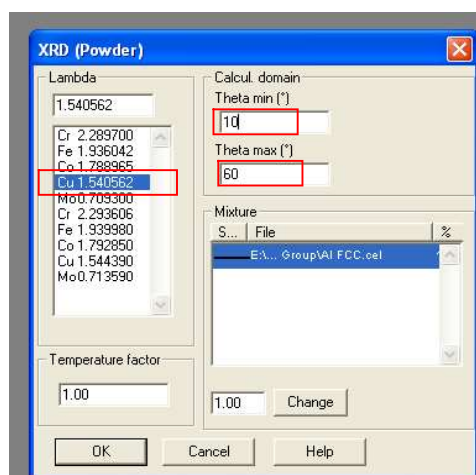


Figure. 4

- Once all the parameters have been specified in step (b), click OK to generate the XRD pattern.
- To save the raw data for the generated XRD pattern, right click on the pattern and select "Save XRD as ASCII file" option. The data file can be exported in ASCII code providing

indexed planes, 2-theta, inter-planar spacing, structure factor, and multiplicity factor. The data file looks like as shown in the next page:

- e. To save the XRD pattern as an image, right click in the window having XRD pattern and select copy. After this, the best way is to paste it in Paint application available in windows OS, and from here the image can be saved in different formats.

The data file after exporting as ASCII code looks like as shown below:

```
CaRine Crystallography 3.0

E:\Back-up_May24-09\Program-files\CaRine Crystallography 3.1\Cells\Pure Elements - Elements\No Space Group\Al FCC.cel
Lambda : 1.540562
Max. value : 147963.656
Number of peaks : 8
(hkl)  2theta  intensity      dhkl  fs2  p
(1 1 1) 38.43   147963.7      2.341 1172.20 8
(2 0 0) 44.67   69435.9 2.027 1026.58 6
(2 2 0) 65.02   39032.4 1.433 672.30 12
(3 1 1) 78.13   41233.8 1.222 508.25 24
(2 2 2) 82.33   11593.8 1.170 464.38 8
(4 0 0) 98.93   5352.0 1.013 326.97 6
(3 3 1) 111.83  18027.6 0.930 253.67 24
(4 2 0) 116.36  17622.6 0.907 233.48 24
```

This ends the instructions for the Part B.

Next, you have been given an Exercise to strengthen your understanding. Solve these exercise questions on the answer sheet provided.

References:

1. *Crystals and Crystal Structures*, R. Tilley, Wiley 2006.
2. *Elements of X-ray Diffraction*, B. D. Cullity, Addison-Wesley 1956.
3. *Solid State Physics*, N. W. Ashcroft, N. D. Mermin, Thomson 1976.

EXERCISE:

Part A: Visualizing different characteristics of a crystal structure e.g. planes, directions, voids etc.

For most of the crystal-structures that you will be drawing, there is no need to change the default lattice parameters, unless mentioned otherwise. Of course you may change the values if it make easier to visualize the structure.

Cubic Crystal:

- 1) Show a unit cell of Cubic Crystal Lattice (Primitive) and Cubic Crystal Structure (Monatomic Basis/Motif).
- 2) In a Cubic Crystal structure, show the following two sets of planes separately. Show by rotating the crystal, the direction along which the two planes in each set intersect. Also, determine these directions. The lattice parameter is $a = 6\text{\AA}$.
 - a) Plane # 1 intersects the axis at $a, a/3, a/4$ and Plane # 2 intersects the axis at $3a, a, 3a/4$.
 - b) Plane # 1 intersects the axis at $2a, 4a, 3a$ and Plane # 2 intersects the axis at $-3a, 3a, \infty a$.

BCC Crystal:

- 1) Show two unit cells of a Body-Centered-Cubic crystal such that they share one plane. Now show an octahedral void.
- 2) Based on the observation in Q. No. 2, find out the effective number of the octahedral voids in a BCC unit cell.

FCC Crystal:

- 1) There are 8 tetrahedral voids in a FCC unit cell. Show any one of them (Hint: The void is surrounded by at least one of the atoms located at the corner of the unit cell)

HCP Crystal:

- 1) Draw a unit cell of Hexagonal Crystal Structure. Now using the **spread of crystal** function, add two unit cells along each of the three axes.
- 2) View this crystal along $[001]$ direction; now the (001) plane as seen on the screen is a closed packed plane. Now, if you want to make a HCP crystal structure, these closed packed planes have to be stacked in a ABAB..... sequence, whereas for FCC these planes are stacked in a ABCABC.... sequence.

Copy the picture of the closed packed plane as seen on the screen into your answer sheet and assuming this is plane A, identify the sites on this plane where the atoms of plane B and C will have to be placed in order to make the above two sequences.

- 3) Draw a hexagonal unit cell. Add an atom at location $1/3a, 2/3b, 1/2c$ in this unit cell; now this modified unit cell is HCP unit cell. Identify and show the two tetrahedral voids in this HCP unit cell.

Slip Plane and Slip Directions:

The edge dislocation plays an important role in plastic deformation of crystalline materials.

Under an external the shear component of the stress causes these dislocations to slip/move in a crystalline material. The plane on which the dislocation line slips are called **slip planes**; these

planes have maximum number of atoms per unit area. The directions along which dislocations slip are called **slip directions**; these directions have maximum number of atoms per unit length.

Now, for Copper (lattice parameter = 3.61 \AA ; calculate the atomic radius yourself):

- 1) Show (111), (110), (100) and (-212) planes. Now, give the answers for Q. No. 2) to 4) in a tabular format.
- 2) Using the software, determine the shortest distance between two atoms in these planes along with the corresponding crystallographic direction. This is the direction with highest packing density of atoms per unit length.
- 3) Calculate the interplanar spacings (d) for these planes (this doesn't require software).
- 4) Calculate the number density of atoms in these planes (# of atoms per unit area of the plane).
- 5) Analyze the numbers obtained for (2) to (4) and predict the slip plane and slip direction.

Part B: X-ray diffraction pattern to determine crystal-structure

- 1) Generate a XRD pattern for a simple cubic crystal s for the 2θ range $10 - 120^\circ$. Assume lattice parameter to be 3 \AA .
- 2) Compare the experimental XRD pattern provided to you in the laboratory with the software generated XRD pattern that was obtained in question No. 1. Based on the difference in the two patterns identify the crystal – structure of the materials for which the experimental XRD pattern has been given to you. [Hint: Use selections rules]
- 3) Using the experimental XRD pattern calculate the lattice parameter.
- 4) Based on the answers in question No. 2 and 3 identify the element that might have resulted in the experimental XRD pattern. You can take the help of following table that shows standard lattice parameter values and crystal structure for various elements [3].

Element	Crystal Lattice	Lattice Parameter (\AA)		Element	Crystal Lattice	Lattice Parameter (\AA)
Ca	FCC	5.58		Mo	BCC	3.15
Ba	BCC	5.02		W	BCC	3.16
Ce	FCC	5.16		Cu	FCC	3.61
Ag	FCC	4.09		Ta	BCC	3.31
Al	FCC	4.05		Tl	BCC	3.88
Pb	FCC	4.95		V	BCC	3.02
Pd	FCC	3.89		Fe	BCC	2.87

- 5) For the element you have identified in Q. No. 4, estimate the crystallite size using the (hkl) peak in the experimental XRD pattern. (hkl values will be informed during the laboratory session).
- 6) Draw three hypothetical FCC unit cells with lattice parameters 1, 2, 3 \AA , and generate corresponding X-ray diffraction patterns in the range (θ) $10-60^\circ$. Notice the position of (111) peak for each. Can you explain this observation?

EXPERIMENT 2

TENSILE PROPERTIES OF MATERIALS

Aim: To conduct a tensile test on Al, Mild Steel and other available materials.

Theory:

Of all the tests used to evaluate mechanical properties, the tensile test, in which a sample is pulled to failure in a relatively short period of time, is perhaps the most useful. In this test (see Figure 1) the sample is elongated at a constant rate, and the load necessary to produce a given elongation is measured as a dependent variable. A load-elongation curve may be plotted from the results of a tension test. These results are usually restated in terms of stress and strain, which are independent of the geometry of the sample.

Engineering stress, σ , is defined as the ratio of the load on the sample, P , to the original cross-sectional area, A_0 :

$$\sigma = \frac{P}{A_0}$$

Engineering strain, ϵ , is defined as the ratio of the change in length of the sample, Δl , to its original length l_0 :

$$\epsilon = \frac{l - l_0}{l_0} = \frac{\Delta l}{l_0}$$

An engineering stress-strain curve for mild steel sample is shown in Fig 2.1.

At the beginning of the test, the material extends elastically; This signifies that if the load is released, the sample will return to its original length. The material is said to have passed its elastic limit when the load is sufficient to initiate plastic, or non-recoverable, deformation; in other words, it will no longer return to its original length if the load is released. (There is always an elastic portion of the total elongation which is recovered,

but during plastic deformation a net elongation remains.) As the sample is further elongated, the engineering stress increases and the material is said to work harden or strain harden. The stress reaches a maximum at the ultimate tensile strength. At this point, the sample develops a neck: this is a local decrease in cross-sectional area at which further deformation is concentrated. After necking has begun, the engineering stress decreases with further strain until the sample fractures. In materials which fracture without necking, the ultimate tensile strength and the fracture strength are the same, but when necking occurs, the load at fracture is lower than the load at the ultimate tensile strength.

The relation between stress and strain in the elastic region is linear for metals and ceramics and is described by Hooke's law:

$$\sigma = E \epsilon$$

where E is a constant, Young's modulus. In metals and ceramics the maximum elastic strain is usually less than one-half of a percent. In rubber and other elastomers, the stress-strain relationship is nonlinear, and recoverable elastic strains of several hundred percent can be produced. The point at which deformation is no longer elastic, but plastic, is that stress at which the slope of the stress-strain curve deviates from the elastic modulus. Because of the difficulty of determining this point precisely, various approximations are frequently used. The most common of these is the offset yield strength, which is usually specified as the stress at 0.2 percent plastic strain.

In low-carbon steels and several other alloys yielding begins at an upper yield point, and the stress then decreases to a lower yield point (see Figure 2.1). This behavior stems from the non homogeneous deformation which begins at a point of stress concentration (often near the specimen grips) and propagates through the specimen in the form of observable bands (Lüder's bands). During elastic deformation there is a slight change in the volume of a metal or ceramic sample; during plastic deformation, however, there is no change in the volume of the sample when measured in the unloaded state. This may be stated mathematically as

$$A_0 l_0 = A_i l_i$$

When a material is elongated, its cross-sectional area must, therefore, decrease. During elastic deformation this change is negligible, but during plastic deformation the reduction in area can be appreciable. It is often preferable for this reason to redefine "stress" and "strain" when considering plastic deformation and to employ the expressions "true stress" and "true strain." *True stress* is defined as the ratio of the load on the sample to the instantaneous minimum cross-sectional area supporting that load:

$$\sigma_T = \frac{P}{A_i}$$

True strain is defined as the ratio of the original cross sectional area of the sample to its instantaneous cross-sectional area and is given by,

$$\epsilon = \ln \left(\frac{A_0}{A_i} \right)$$

When the increase in stress necessary to continue deforming the material is finally counterbalanced by the increase in applied stress due to the decreasing cross-sectional area, the material necks, or starts to deform locally at decreasing loads. In many metals, work-hardening occurs in an approximately parabolic manner, which may be expressed as.

$$\sigma_T = K \epsilon^n$$

where K is a constant and n is the work-hardening exponent (always less than one). In materials necking begins when the true strain is equal to the work-hardening exponent. The results of the tensile test are extremely useful to the designer. In most engineering structures only elastic deformation is desirable. A knowledge of the yield strength thus establishes the maximum load that can safely be employed (which is then usually reduced by a safety factor). Many techniques of fabrication, such as rolling, wire drawing, and stamping, depend on the ability of a metal to withstand appreciable plastic deformation prior to fracture. Here it is important to know the ductility and rate of work-hardening of

the material being worked. The area under the stress-strain curve in the tension test shows the energy absorbed before fracture and thus indicates the *toughness* of the material.

Specimen Geometry:

Typically a plate or cylindrically shaped specimens are used in tensile test. The test specimen has a uniform cross section, which ensures that the deformation is confined to the narrow gauge section. The specimen is mounted at its ends by grips of tensile testing equipment.

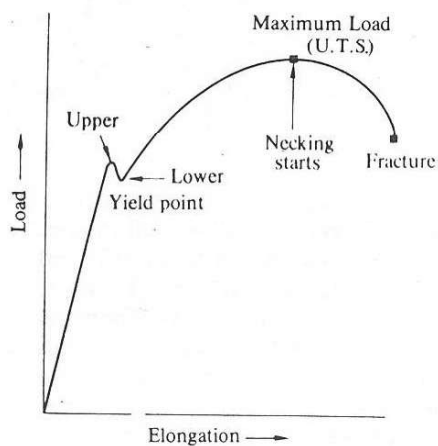


Fig .2.1 A Load Vs Elongation curve showing yield point phenomenon

Procedure:

In this experiment specimens of commercially available pure Al and mild steel will be tested under tension using Hounsfield tensometer. In general, the experimental procedure for any testing machine would involve measurement of original length and diameter of the specimen. The length may either be the length of gauge section which is marked in the specimen with a preset punch or the total length of the specimen. Insert the specimen into grips of the test machine and attach a strain-measuring device to it. Begin the load application and record load versus elongation data.

Take readings more frequently as yield point is approached. During the initial stages of plastic deformation the load rises rapidly. Later on when necking is approaching, there is a large amount of extension for a small increase in the applied load.

The elongation values are then measured with the help of dividers and a ruler. In Hounsfield Tensometer the elongation is recorded on a moving graph paper. Continue the test till fracture occurs. By joining the two broken halves of the specimen together, the final length and diameter of the specimen can be measured.

Observations:

1. Record the data in the following table.

Material :

Original dimensions Final dimensions

Length : Length :

Diameter : Diameter :

Load	Engineering Stress	Elongation	Strain	True stress	True Strain
Kg	Kg/mm ²	mm	mm/mm	Kg/mm ²	mm/mm

2. Calculate per cent elongation at fracture, per cent reduction in area at fracture, yield strength (or 0.1 per cent proof strength) and ultimate tensile strength for the given materials.

3. Plot a true stress Vs true strain curve for one of the specimens from the tensile data.

4. Calculate the modulus of elasticity with the help of stress-strain diagram.

Questions:

1. Explain the absence of pronounced yield point in aluminum specimen?

2. How does the presence of carbon influence the strength of steels?

3. Can u calculate the work done in deforming a specimen with the help of available tensile data?

Experiment 3

Microstructures of Steels and Cast Irons

Aim: To study the decomposition of austenite as a function of cooling rate

Theory :

Introduction

Heat treatment is used to change the mechanical properties of metal by suitable alteration of its metallurgical structure. Usually the primary purpose of heat treatment is to increase the strength of metal while retaining some toughness or ductility, but heat treatment is also employed to soften a metal to facilitate machining, to allow easier forming, or for other purposes. Mechanical properties are controlled by the micro constituents of the metal. The nature, shape, amount, and distribution of the constituents are controlled by heat treatment to provide structural configurations that have mechanical properties suitable for the intended use. The words "heat treatment" are general, and indicate that a heating and cooling cycle has been performed on metal to alter its properties in some manner. Although these words bear the connotation to some engineers and metallurgists that only steels are being considered, such an interpretation is too narrow, and heat treatment may be applied to many nonferrous alloys as well as to steels.

Iron-Carbon Phase Diagram

The iron-carbon phase diagram shown in Fig. 7-1 indicates the phase changes that occur during heating and cooling and the nature and amount of the structural components that exist at any temperature. The high-temperature phase, called austenite, decomposes on cooling. This phenomenon, in which a solid transforms in a eutectic manner, is called a eutectoid transformation, with E being the eutectoid point and the composition at E the eutectoid composition. During ordinary heat-treating operations, steel is seldom heated above 1800°F; thus it is possible to simplify the study of the phase diagram by not considering at this time the portion above that temperature. Below 1800°F, the equilibrium structures include austenite, ferrite, cementite, and pearlite. In as much as the properties of the final product depend upon the properties of individual constituents, the nature and properties of each component are first considered separately .

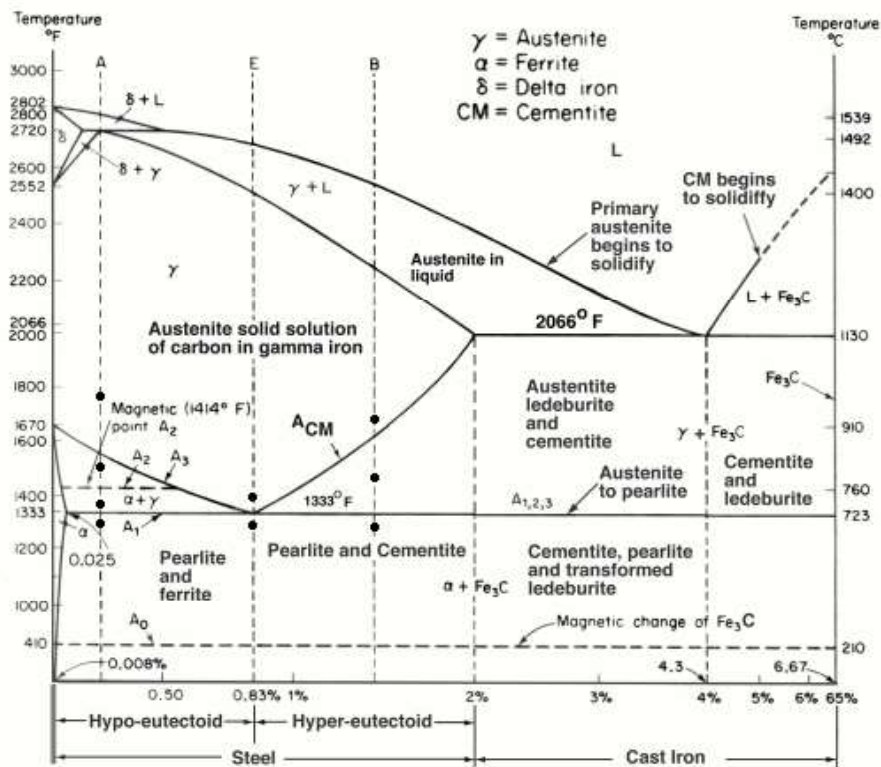


Fig. 7-1 Iron-Carbon equilibrium diagram (Adapted from Metals Handbook, ASM)

Austenite

Austenite is a soft and ductile phase consisting of carbon dissolved in gamma iron, the face-centered cubic polymorph of iron. Maximum solubility of carbon in austenite is 2.0% at 2066°F. It is evident from the phase diagram that austenite can only exist at elevated temperatures in plain carbon steel, but in some highly alloyed steels austenite is banded by prior mechanical working. A typical room-temperature austenite structure is shown in Fig. 7-2.



Fig 7.2 Microscopical appearance of austenite. Photograph is of 18%Cr-8% Ni stainless steel in which the austenite is stable at room temperature. Chromic acid etched. X 100

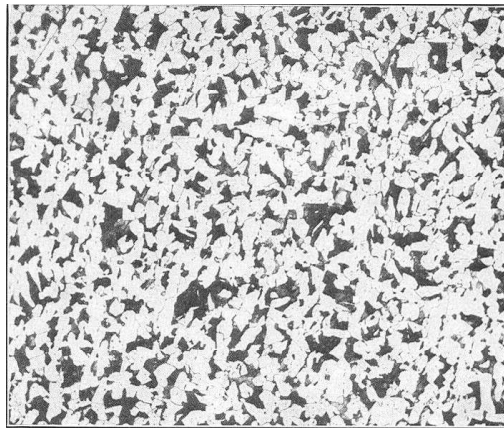


Fig 7-3 Microstructure showing ferrite and pearlite

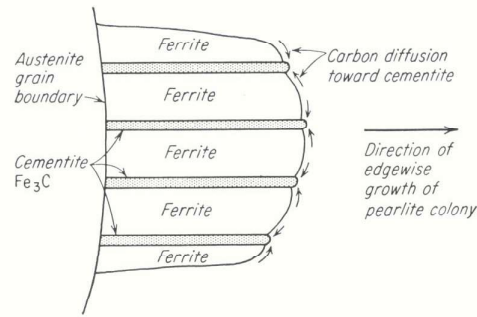


Fig 7-4 Diagram of pearlite growth colony in austenite. Carbon diffuses through austenite forming cementite plates which grow edgewise

Ferrite

Ferrite is the name given to solid solutions in which the solvent is alpha iron, the body-centered cubic form of iron, and the solute is principally carbon, perhaps with minor amounts of manganese, silicon, and other alloying elements commonly present in steel. Since the major alloying element, carbon, is soluble in amounts not greater than 0.025%, ferrite is often described as being "nearly pure iron." Ferrite is the softest constituent of steel and is very ductile. The microstructural appearance of ferrite is shown in Fig. 7-3.

Cementite

The hardest constituent of steel is iron carbide (Fe_3C), having approximately 650 Brinell hardness. Unfortunately, this hard compound, called cementite, is also extremely brittle. Because its carbon content (6.67%) is much above the 2.0% maximum carbon content of steel, cementite can never be the sole constituent of steel. It is always accompanied by other lower-carbon constituents, probably ferrite or pearlite.

Pearlite

Pearlite is a lamellar structure of alternate plates of cementite and ferrite, and as a mechanical mixture of two phases it has properties intermediate between those of its components. It is softer and more ductile than cementite, but harder and stronger than ferrite. Pearlite has its characteristic and easily recognizable lamellar appearance because of its habit of growth. During slow cooling of austenite, nuclei of cementite form at the austenite grain boundaries and grow into platelets by edgewise growth into the austenite matrix. This type of growth is illustrated in Fig. 7-4. The carbon content of cementite is much higher than the carbon content of austenite, and carbon must diffuse through the

austenite toward the growing cementite plates. Austenite adjacent to the growing cementite plate is depleted of carbon and transforms to ferrite. Areas of pearlite are nucleated at austenite grain boundaries and grow by consuming the parent austenite. When the carbon content of the austenite is depleted so that no further cementite can be formed, the remaining austenite transforms to ferrite. At low magnification, pearlite appears dark, but the higher magnification photograph shows both cementite and pearlite as light-etching constituents. When the alternate plates of cementite and pearlite are so close together that the microscope is unable to resolve the structure, pearlite appears dark because of the differences in level of the cementite and ferrite laminations caused by the etchant.

When steel is rapidly cooled (quenched), insufficient time is allowed for the necessary atomic movement to be completed at the elevated temperature. At lower temperatures the atomic mobility of the metal is so drastically reduced that the same change cannot take place. A new type of reaction then occurs in which austenite does not transform to coarse pearlite with an excess of ferrite or cementite, but changes to structures called bainite or martensite. Combinations of these structures are common.

Fine Pearlite

As its name indicates, fine pearlite is a lamellar pearlitic structure in which the individual plates of ferrite and cementite are much thinner than in the pearlite formed during slow cooling of austenite. When cooling is rapid, more cementite plates are nucleated, and individual lamellae of pearlite become thinner until they are practically unresolvable by even the best microscopical methods. However, there is no indication of any marked change in the mode of formation and lamellar plates do exist. The resulting structure is called fine pearlite and is considerably stronger and harder than coarser pearlite formed by slow cooling.

Martensite

When the quenching rate is sufficiently rapid to prevent transformation of austenite above approximately 600°F, martensite forms on further continuous cooling. Martensite is quite hard and strong, but also is brittle. It is a supersaturated solution of carbon in ferrite, and the presence of the excess carbon distorts the normally cubic ferrite to a tetragonal cell, which is strained and therefore hard and strong. The mechanism of

formation of martensite is entirely different than for the other structures present in steel. Martensite plates form by a shearing action along crystallographic planes rather than by diffusion of atoms through the solid metal, as in the case of ferrite and cementite. This shearing action takes place very rapidly and cannot be suppressed by rapid cooling. For a given alloy, martensite begins to form at a particular temperature and continues to form as the temperature is lowered, until all the austenite has transformed to martensite. It is necessary to cool some metals below room temperature to obtain a completely martensitic structure and eliminate the last vestiges of "retained austenite." Individual martensite plates are lenticular in shape, and are generally quite small; thus they may not be well resolved for microscopical examination. The usual appearance of martensite is as shown in Fig. 7-5

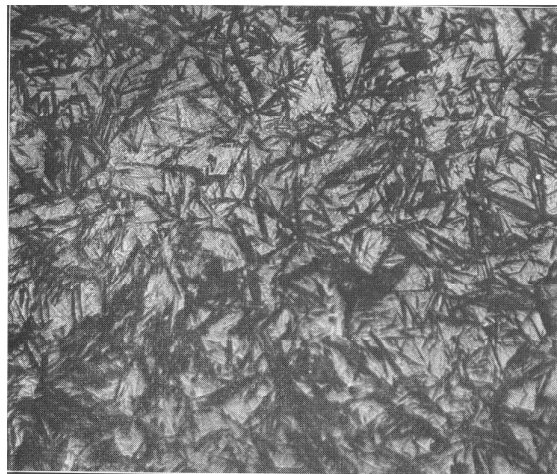


Fig 7-5 Typical microscopical appearance of martensites in hardened steel .1.3 % carbon
Etched with 2% Nital X500

Bainite

Between the temperature range where pearlite forms and that where martensite forms, it is possible for austenite to transform to a structure called bainite. As in the case of pearlite, bainite forms by a nucleation and growth process which takes time and can thus be suppressed by rapid cooling. (Fig 7-6) The appearance of bainite varies considerably, being coarse and feathery when formed toward the upper end of the transformation range, and considerably finer and acicular in appearance when formed toward the lower end of the range. Bainite in plain carbon steels is usually formed by constant temperature transformation of austenite. Austenite is quenched to a temperature

within the bainitic range and held at the quenching temperature for a sufficient length of time to allow complete transformation to occur. However, some alloy steels form bainite during continuous cooling to room temperature. This will be more evident from the following discussion.

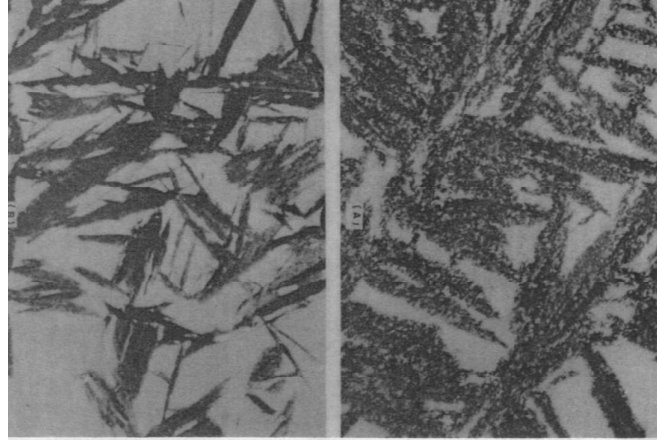


Fig 7-6 Microstructure of Bainite

Time and Temperature in the Transformation of Austenite

It has been previously indicated that austenite transforms to ferrite and cementite on slow cooling and to fine pearlite, bainite, and martensite when more rapidly cooled. Since the purpose of heat treatment is to obtain metallographic structures that have the desired properties, it should be possible to predict accurately the structure formed by any heat treating cycle. Although the iron-carbon phase diagram is a necessary adjunct to such prediction, it is not notably useful for non equilibrium transformation of austenite. Non equilibrium transformation can best be described with the aid of the time-temperature-transformation curves, and the continuous-cooling curves which are modified TTT curves. The TTT curves indicate the time required for austenite to transform at any constant temperature. The type of structure formed is also indicated (see Fig 7-7.). Continuous-cooling curves are somewhat similar to TTT curves, but as the name implies, are based on transformation of austenite during continuous cooling rather than transformation at constant temperature. Primarily, TTT diagrams are used in predicting the metallographic structure and mechanical properties of steel samples

quenched from the austenite region and held at constant elevated temperatures below 1330°F. If a sample of the steel whose diagram is rapidly cooled to 1100°F and held at that temperature for approximately 2.5 sec, ferrite begins to form. After 8 sec the ferrite transformation ceases and pearlite formation begins, and continues until the transformation of austenite is complete after 100 sec.

If the same steel is quenched from 1450°F to 600°F, no ferrite or pearlite obtained, but after 19 sec bainite starts to form. At approximately 1,000 sec the structure is 100% bainite. In both of these cases, transformation of austenite has occurred at constant temperature. If the steel is quenched from 1450°F to 375°F, other mode of austenite transformation is introduced. Martensite gins to form at 500°F and at the quenching temperature approximately % of the austenite becomes martensitic. On holding at 375°F, no change occurs until approximately 2,000 sec have passed, when the remaining austenite begins to form bainite. The bainitic transformation is complete after 1 day, giving a final structure of approximately 40% martensite and 60 % bainite.

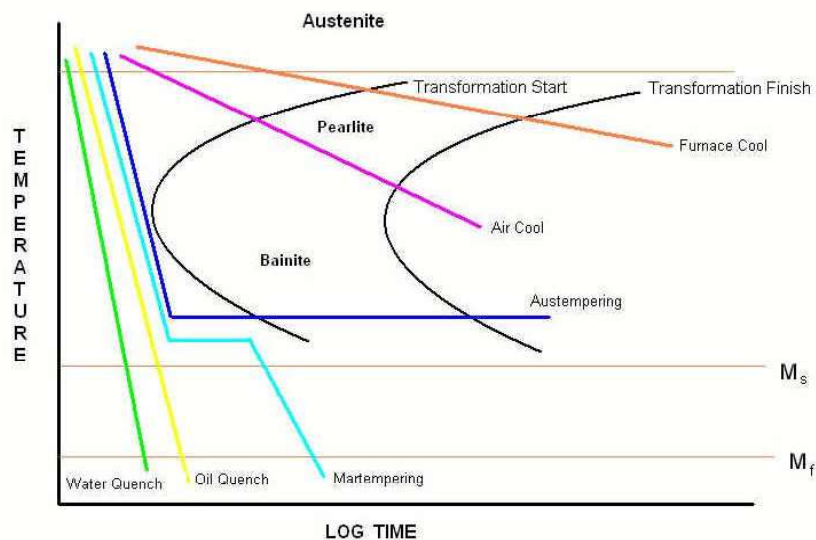


Fig 7-7 TTT curves

Equipment

About six specimens of a 0.8 per cent carbon steel. One furnace each at the following temperatures: 950, 200, 400, and 700°C. Bucket of water. Polishing and etching equipment. Metallurgical microscope. Rockwell hardness tester.

Observations

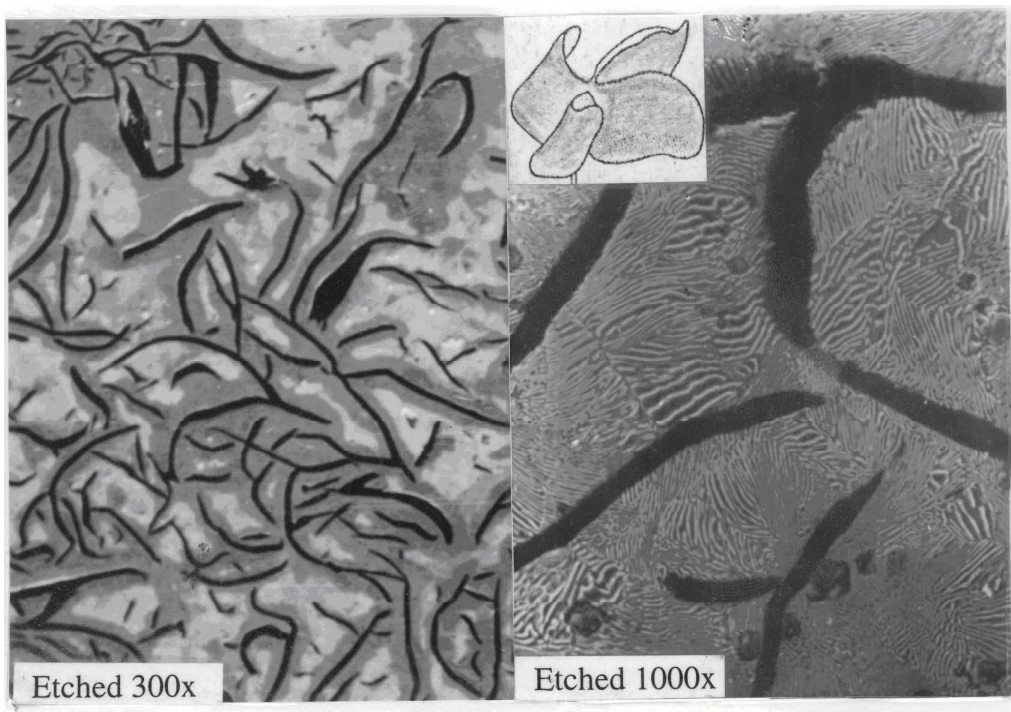
1. Describe the microstructures obtained in each case.

Questions

1. How does the hardness vary with cooling rate?
2. How do your microstructures compare with standard microstructures of coarse pearlite, fine pearlite and martensite?
3. How does hardness vary with tempering temperature? How do you explain this variation?
4. Why is it necessary to be really quick in transferring the specimen from the austenitizing furnace to the water bath during quenching?

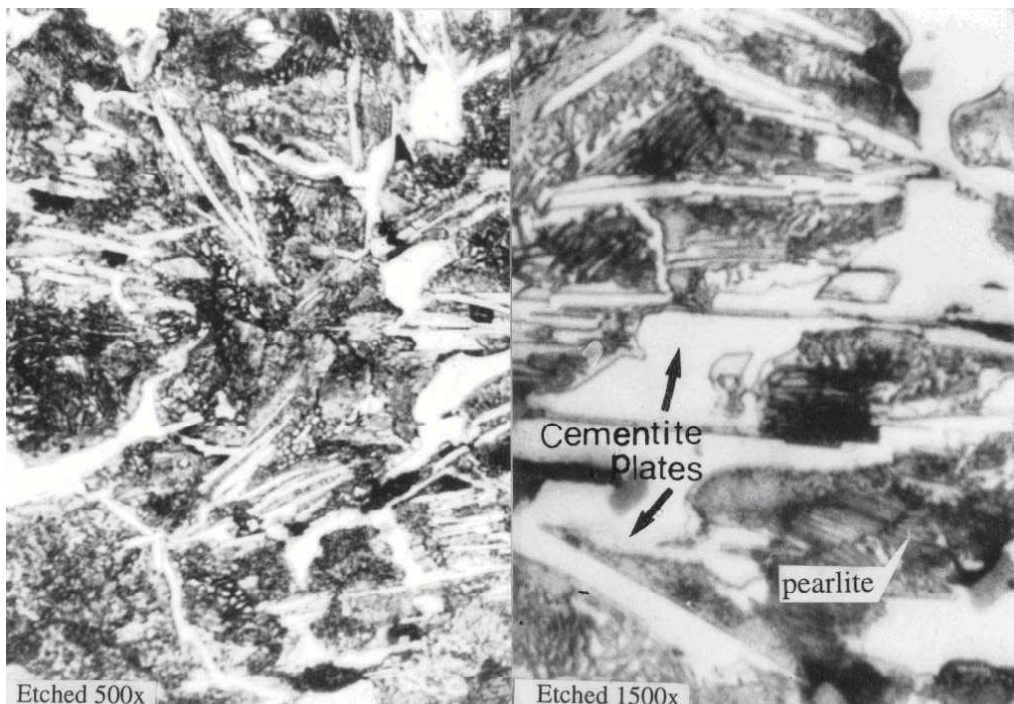
Gray cast iron

When a cast iron is solidified slowly, the tendency of carbon to separate out as graphite increases. In gray cast iron, the graphite precipitates as irregular, elongated, curved and interconnected plates. Although the flakes appear as if separated in the two-dimensional microstructure, they are interconnected in three dimensional structures (inset). The large graphite flakes not only interrupt the continuity of the matrix but also act as stress risers. As a result, the strength and ductility of the gray cast iron decreases. However, the presence of flake graphite provides good wear and thermal properties along with good damping capacity. Gray cast iron is widely used for gear and pump housings, machine beds, brake drums, motor frames and electrical equipment.



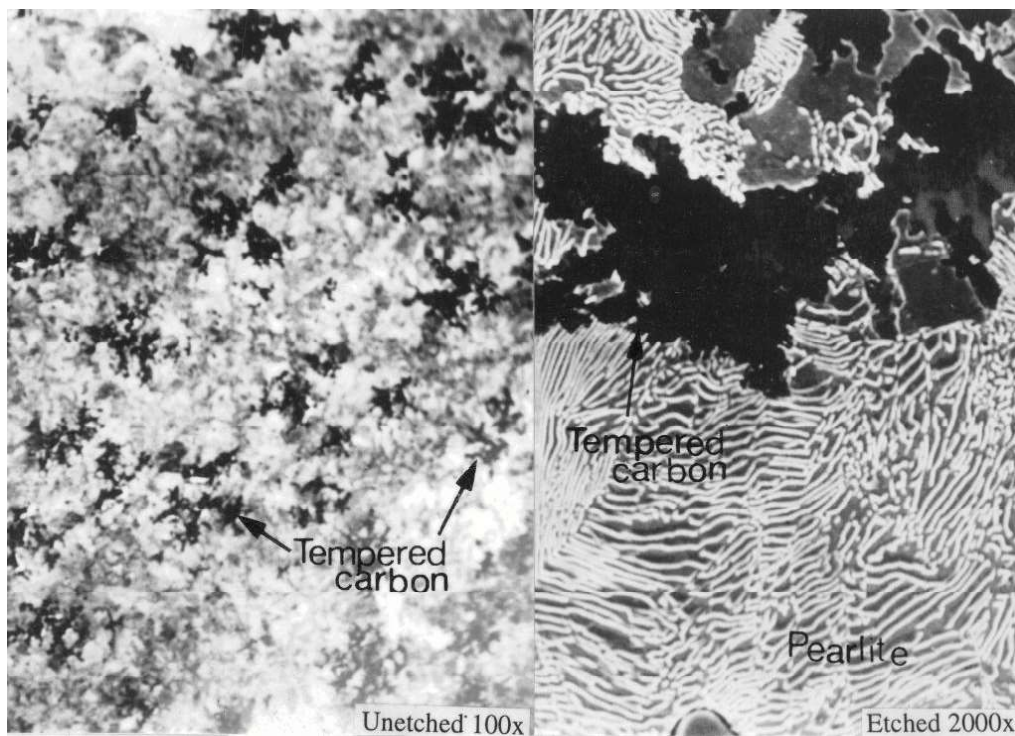
White cast iron

White cast irons are hypo eutectic alloys and form a eutectic mixture of austenite and cementite (known as ledeburite) upon cooling. A typical microstructure of white cast iron consists of dendrites of transformed austenite (later to pearlite) in a white interdendritic network of cementite. Cementite is a hard, brittle interstitial compound. Since white cast iron contains relatively large amounts of cementite as a continuous interdendritic network, it makes the white cast iron 'hard' and 'wear resistant', but extremely brittle and difficult to machine. Completely white cast irons are limited in engineering applications because of inherent brittleness and lack of machinability. They are used where wear resistance is most important and the service does not require ductility such as liners for cement mixtures, ball mills, certain type of drawing dies and extrusion nozzles. White cast iron is also a starting material for malleable cast irons.



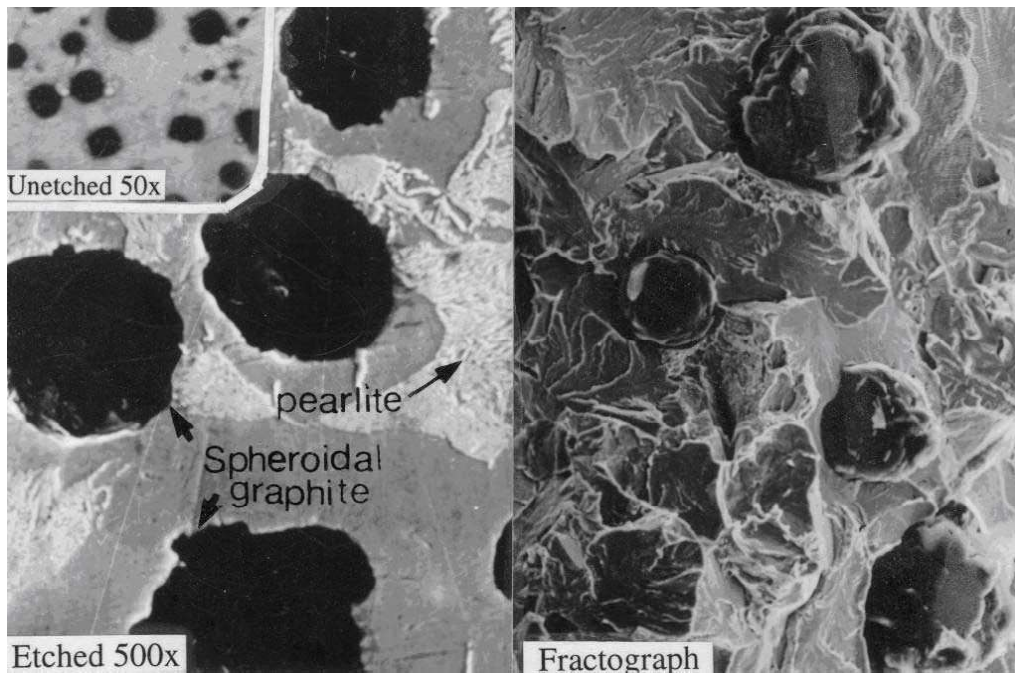
Malleable cast iron

In white cast irons, carbon exists as combined carbon (cementite). As you are aware, Cementite is a metastable phase. Under normal conditions it persists in its original form, however, upon prolonged heat treatment cementite decomposes into iron and carbon ($\text{Fe}_3\text{C} \sim 3\text{Fe} + \text{C}$). This reaction normally occurs at elevated temperatures and it is further assisted by non-metallic impurities, higher carbon content and the presence of certain alloying elements. The decomposition process of cementite to carbon is known as malleabilization. The decomposed carbon nucleates at different places, grows in all directions and ultimately appears as irregular nodules (referred as Tempered carbon). As a result of tempered carbon formation (brittle cementite is replaced with softer phases) cast iron obtains higher strength and ductility. Malleable iron is widely used for automotive, agricultural and machine parts. Because of long heat treatment cycles involved it is not really cost effective hence it is now being replaced by spheroidal graphite cast iron.



Spheroidal Graphite cast iron

Spheroidal graphite cast iron (also known as nodular graphite cast iron or ductile iron) is a cast iron in which the graphite is present as tiny balls or nodules (see the fracture surface). The spheroids interrupt the matrix less than graphite flakes and this results in higher strength and toughness compared to gray cast iron. Unlike malleable iron (where long heat treatment is required) ductile iron is produced by treating low sulphur iron with Mg or Ce. Some typical application of nodular iron include crank shafts, pistons, cylinder heads, fly wheels, work rolls, lever etc.



Experiment No. 04

Dielectric Behavior of Barium Titanate

Dielectrics are a class of materials that do not conduct and are used as insulators.

Another important use of these materials is as capacitors, or even transducers.

In conductors, in response to an electric field, the charges move freely over a long distance. In dielectrics, there are no free charges, or at least in the ideal ones there aren't any. So, we may be tempted to ignore the issue of charges in this class of materials when a field is applied. However, Faraday discovered that something did happen when a dielectric material was inserted, say, between two parallel plates of metal. That, story you already know well. We must therefore look into the response of charges to electric field in dielectrics also, though they may be bound.

From the experience of every day life, if you are not already convinced about the importance of dielectrics, in spite of living in electronic age, just look inside the CPU of your computer (you may need an SEM!). The large scale integration of devices is only possible because of high dielectric constant insulators that form miniaturized capacitors and low dielectric constant insulators that separate two devices from each other.

With electric flux density:

$$\mathbf{D} = \epsilon_0 \mathbf{E} + \mathbf{P} \quad (1),$$

and polarization expressed as

$$\mathbf{P} = \epsilon_0 \chi \mathbf{E} \quad (2),$$

where,

D: electric flux density, a defined quantity

E: fundamental field, the electric field

P: polarization, expressing response of a material in an electric field

χ : dielectric susceptibility.

Accordingly, consistent with the relationship

$$\mathbf{D} = \epsilon_0 k \mathbf{E}, \quad (3)$$

from (1)-(3), we have

$$k = \chi + 1, \quad (4)$$

where k is the dielectric constant, though not always independent of the electric field.

What is explained above is a macroscopic approach you are well familiar with from probably the school days. In order to look into the materials, it is necessary to take a microscopic approach, for which we introduce a quantity called polarizability, defined as

$$\alpha = \frac{\mathbf{P}}{N E_{\text{Loc}}} \quad (5)$$

where, N is the number of dipoles in a unit volume and E_{Loc} is the local electric field, when the external field applied is E . For example, in dilute gases, the local and applied fields are the

same, and for materials of cubic symmetry, $E_{\text{Loc}} = E + \frac{\mathbf{P}}{3\epsilon_0} = \frac{E}{3}(k + 2)$. In general, therefore,

we will write

$$E_{\text{Loc}} = E + \beta \frac{\mathbf{P}}{\epsilon_0} \quad (6).$$

You already know what dielectric constant is, but the nature of polarization on application of electric field leads to two kinds of dielectrics: linear and non-linear (ferroelectric, among others) dielectrics. Barium titanate belongs to the latter class.

Barium Titanate as a Dielectric

BaTiO_3 at temperatures above 120°C exhibits a perovskite structure as shown in figure 1. The lattice is a simple cubic, with basis as one Ba^{2+} ion at $(0,0,0)$, one Ti^{4+} ion at $(\frac{1}{2}, \frac{1}{2}, \frac{1}{2})$ and three O^{2-} ions at $(\frac{1}{2}, \frac{1}{2}, 0)$, $(\frac{1}{2}, 0, \frac{1}{2})$ and $(0, \frac{1}{2}, \frac{1}{2})$. Find ionic radius of oxygen and titanium. Your estimate of ratio of the cation to anion radius should come out to 0.468. That suggests, the coordination of the Ti^{4+} will be octahedral, consistent with the perovskite structure.

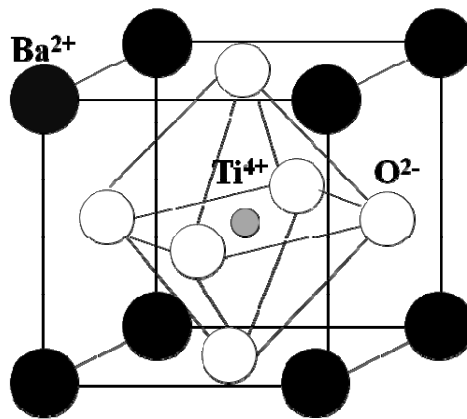


Figure1: Crystal Structure of Barium Titanate above 120°C

The Ti^{4+} ion residing in the middle is small; therefore, in an open structure, it is relatively free to move. Also, the structure is centrosymmetric. Thus, the centers of positive and negative charges coincide and no polarization exists in absence of a field. But, when a field is applied, because the Ti ion is relatively free to move, a large polarization develops. This is the picture above 120°C . But, what happens as you cool down this material?

Let us look at it mathematically first. Combining (5) and (6) yields,

$$P = N\alpha \left(E + \beta \frac{P}{\epsilon_0} \right) \text{ or after rearranging,}$$

$$\left(1 - \frac{N\alpha\beta}{\epsilon_0}\right)P = N\alpha E \quad (7)$$

which upon using the definition in (2) derives susceptibility as

$$\chi = k - 1 = \frac{N\alpha}{\epsilon_0 \left(1 - \frac{N\alpha\beta}{\epsilon_0}\right)} = \frac{N\alpha}{(\epsilon_0 - N\alpha\beta)} \quad (8)$$

Now, what would happen when $\frac{N\alpha\beta}{\epsilon_0} \rightarrow 1$? Humm..interesting, isn't it?

Let us start again. Suppose we start with temperatures well in excess of 120°C. The electric field will try to align the dipoles. But, high thermal energy will randomize the direction of dipoles, with a net result that values of P or α are small (when they are zero, $k=1$ and $\chi=0$) and the ratio $\frac{N\alpha\beta}{\epsilon_0}$ is small. When the temperature begins to decrease, with the reducing thermal impact, the polarization, and thus, $\frac{N\alpha\beta}{\epsilon_0}$, increases, causing susceptibility and dielectric constant to also increase. Eventually, as this ratio, $\frac{N\alpha\beta}{\epsilon_0}$, approaches unity, the χ , k and P must shoot up to infinity. What is the implication of dipole moment shooting up too high? It means that the crystal will fly off apart. Hence, if barium titanate has to exist, something must happen. That something happens at 120°C. The crystal undergoes a phase transformation to a tetragonal structure.

On cooling below 120°C, one of the cubic edges becomes elongated so that the material assumes tetragonal symmetry ($a=b \neq c$; $\alpha=\beta=\gamma=90^\circ$). At room temperature $c/a=1.01$ i.e. c-axis has elongated by 1 percent. The titanium ion is centrally located with respect to six surrounding oxygen ions in the cubic phase. The equidistant tetragonal distortion produces a perturbation in

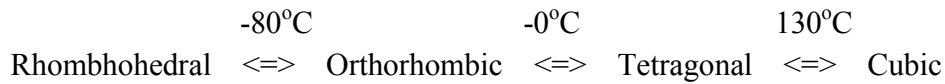
the crystalline potential within the unit cell so that the titanium ion, instead of remaining equidistant from the two oxygen ions in the c-direction, moves closer to either oxygen ion. This non-centrosymmetric location of the titanium ion sets up a permanent dipole and causes spontaneous ionic polarization.

Let us understand this in simpler terms. Imagine you had cubic BaTiO_3 as indicated in figure 1. Now to obtain a tetragonal structure, you are squeezing in a- and b- directions, while c-axis is being elongated. The central Ti^{4+} , which now feels the squeeze from those 4 oxygen ions in the a-b plane, pops up or down in the c-direction. That final picture of atomic locations can be seen in figure 2. What is important is that now the structure is not centrosymmetric, that center of positive and negative charges are not the same. This implies that even in the absence of an electric field, a unit cell of BaTiO_3 shows a dipole moment and hence polarization in the c-direction. What is also interesting is that if Ti^{4+} in one unit cell moves up or down, the neighboring unit cells follow cooperatively to yield a large dipole moment together.

When the direction of the spontaneous polarization of a material can be reversed by the interaction of the electric dipole moment of the atoms with an external applied electric field, the material is said to exhibit ferroelectric behavior and the phenomenon is called ferroelectricity.

All ferroelectric materials have a transition temperature, called the Curie point (T_c). At a temperature $T > T_c$, the crystal does not exhibit ferroelectricity, while for $T < T_c$, it is ferroelectric. On decreasing the temperature through the Curie point, a ferroelectric crystal undergoes a phase transition from a non-ferroelectric (paraelectric) phase to a ferroelectric phase.

Finally, Barium Titanate, BaTiO_3 , exhibits additional polymorphic transformations, which are indicated below.



In this experiment, you are to observe the cubic to tetragonal phase transformation in barium titanate.

Equipment Available

1. A heating stage
2. Capacitance Meter

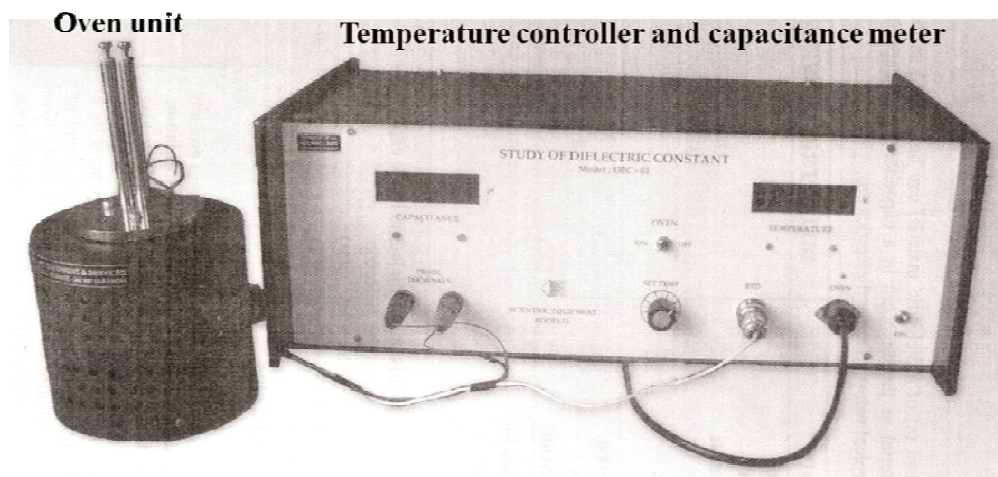
Preparation for the Experiment

On a sheet of paper, write your response to following pointers. Discuss them with your tutor/TA, only then begin the experiment.

1. What is the objective? State it crisply.
2. In order to meet the objective, what will be the experiment design? Meaning, what will you vary (independent variable) and what will you measure (the response).
3. What will be range of independent variable? What will be the interval in which you will vary the independent variable? Will it be the same throughout the range, or will you be changing it? If you decide to vary the interval, how will you decide when to change that interval and to what value?
4. At what rate (in time) will you change the independent variable?
5. Post measurements, what will you do with the data? Are you going to do any further calculations and/or are you going to make a plot and then do analysis? State them.

6. If you are going to do some calculations with the data you record in a table, how many columns (and their title) you will require in the table? Do you require any data to do those calculations?
7. In case of a plot, what kind of graph paper you require?

Equipment Connections



Experimental set-up

Questions

- 1) What factors contribute the difference between experimental and theoretical value of Curie temperature? (Try to elucidate on the basis of impurity, ambient temperature, geometry of sample etc.)

EXPERIMENT 5

Thermal Analysis of Pb-Sn Alloy

Aim: To produce thermal cooling curve and report eutectic temperature.

Theory:

Phase Diagrams

Phase diagrams, sometimes called equilibrium diagrams, are graphs that indicate, for a particular alloy system, the phases that are present at any temperature, with various compositions. The coordinate system of phase diagrams uses temperature as the ordinate scale and weight percentage of the alloy components as the abscissas. The particular temperatures at which phase changes occur are plotted on this diagram for a given alloy composition, and when sufficient experimental points have been determined, lines representing the locii of all phase changes are drawn. These lines are also the boundaries of various phase fields. With the complete phase diagram the phase or phases existing at any temperature or the phase changes occurring on changing temperature can be easily determined for any alloy of the two elements. The phase diagram is also valuable for determining the percentage amount of a particular phase in a two-phase structure, and it assists in understanding phenomena that occur during rapid heating and cooling. (Fig 9-1) Since most metallurgical operations are completed well below the boiling temperature of the various components of the alloys and at normal atmospheric pressure, vapor phases and the effect of pressure are ordinarily not considered.

Constructing Phase Diagrams

Data for constructing phase diagrams may be obtained by several methods. Thermal analysis, microscopical studies, and X-ray diffraction are common. Thermal analysis is the simplest and most used technique. By slowly heating or slowly cooling alloys of known composition while accurately measuring the temperature of the alloy at particular time intervals, plots are obtained which show the variation of temperature with time. Any departure from a smooth curve is an indication of a phase change at the inflection temperature. During the freezing of a pure metal, the latent heat of solidification which is liberated is exactly sufficient to maintain the alloy at constant

temperature until freezing is complete. A constant-temperature dwell appears in the cooling t curve. Latent heat liberated during the freezing of a solid-solution alloy is not sufficient to maintain constant temperature, but does decrease the rate of cooling, as seen in Fig. 9-3.

By obtaining cooling curves for several particular compositions of the alloy system being investigated and plotting the inflection temperatures of each cooling curve against the alloy composition, points which indicate regions of phase changes are obtained. Lines representing the loci of phase changes are then drawn, and the lines become the boundaries of phase fields. Fig. 9-2

The thermal-equilibrium diagram is in reality a chart which shows the relationship between the composition, temperature and structure of any alloy in a series. Let us consider briefly how these diagrams are constructed.

A pure metal will complete its solidification without change of temperature whilst an alloy will solidify over a range of temperature which will depend upon the composition of the alloy. Consider, for example, a number of alloys of different composition containing the two metals A and B which form a series of solid solutions (Fig. 9.2). For successive compositions containing diminishing amounts of the metal A, freezing commences at a_1 , a_2 , a_3 , etc., and ends at b_1 , b_2 , b_3 , etc. Thus, if we join all points' a_1 , a_2 , a_3 , etc., we shall obtain a line called the liquidus, indicating the temperature at which any given alloy in the series will commence to solidify.

Similarly, if we join the point's b_1 , b_2 , b_3 , etc., we have a line, called the solidus, showing the temperature at which any alloy in the series will become completely solid. Hence the liquidus can be defined as the line above which all indicated alloy compositions represent completely homogeneous liquids, whilst the solidus can be defined as the line below which all represented alloy compositions of A and B are completely solid. For temperatures and compositions corresponding to the co-ordinates of points between the two lines both liquid solutions and solid solutions can co-exist in equilibrium.

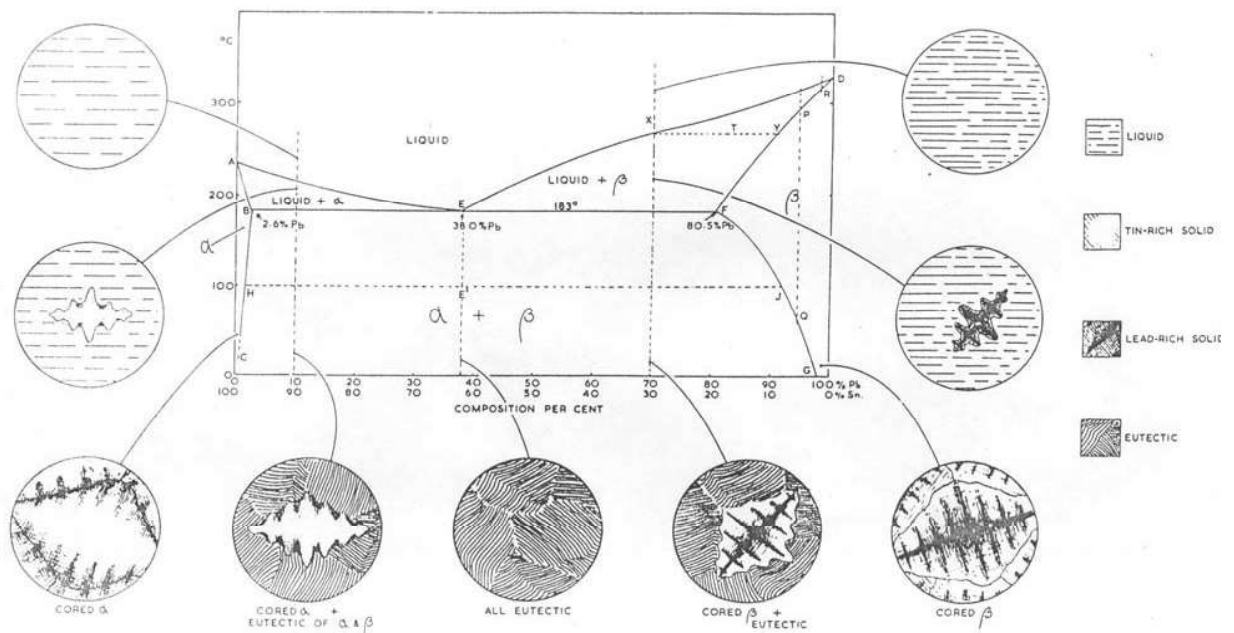


Fig 9-1 The tin-lead equilibrium diagram. The microstructures indicated are those obtained under *non-equilibrium* conditions of solidification

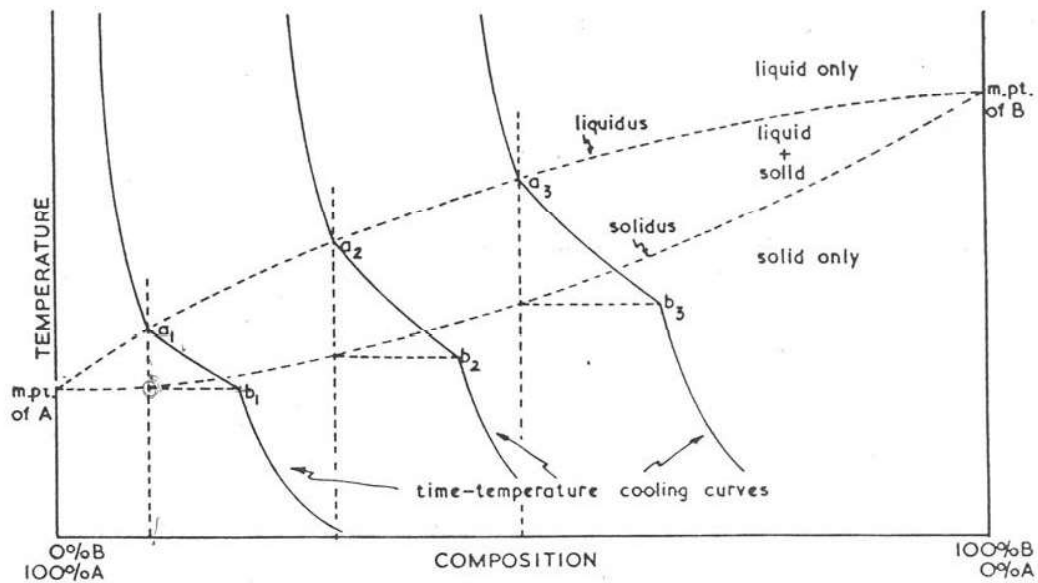


Fig 9-2 The construction of a simple equilibrium diagram of the solid solution type using cooling curves of a series of alloys

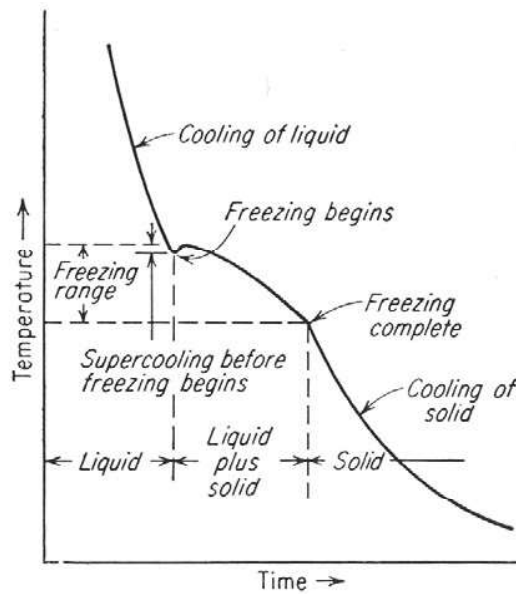


Fig 9-3 Cooling curve of a solid-solution alloy.
Discontinuous changes in slope of cooling curve indicate phase change

Pure metals cool relatively uniformly to their freezing temperature and then remain at the freezing temperature until solidification is complete. If doubt exists that a particular sample is pure metal, chemical analysis or X-ray diffraction technique may be utilized to provide indisputable evidence.

Solid solution alloys are microscopically indistinguishable from pure metal but melt over a temperature range rather than at a constant temperature. X-ray diffraction measurements also indicate the presence of a solid solution through a change of their lattice parameter compared to the pure components. These and other indications prove the presence of a solid solution alloy.

Equipment:

Fire clay crucibles, Chromel –Alumel thermocouple, furnace with variac, potentiometer for reading thermocouple, Pb-Sn sample.

Procedure:

1. The molten alloy is kept in crucible in the center of the furnace.
2. Immerse Chromel-Alumel thermocouple with protective sheath into the molten metal.

3. The current through the furnace is to be adjusted so that we will get 1 or 2 °C per min.
4. Temperature readings for every 1 min has to be recorded using potentiometer.
Be sure that you make any necessary reference junction corrections.

Observations:

Time Min	Temperature °C	

Questions:

1. Estimate the composition of your sample.
2. Compare the direct and inverse cooling curves
3. Discuss the arrest point in Pb-61.9 % Sn Alloy.
4. What type of binary system is represented by Pb-Sn alloy?

Experiment 6

Thermal Expansion of Solid Materials

Aim:

To study the thermal expansion behaviour of solid materials using a dial gauge dilatometer.

Theory :

Almost all materials expand on heating. This can be understood in terms of the potential energy curve. Consider a pair of atoms, bound together in the solid. The potential energy, $V(r)$, of these two atoms varies with their separation, r , and can be represented by

$$V(r) = -a/r^m + b/r^n \quad (11.1)$$

where a , b , m , and n are constants, and are positive quantities. The first term on the right arises from the attraction between the two atoms (decreasing r lowers the energy); the second term comes from repulsion. These two terms are shown as dotted lines in Fig. 11.1 and the total potential energy by a solid line. The asymmetric shape of the potential energy curve may be noticed. The degree of asymmetry is a function of the values of the exponent's m and n in equation. (11.1) m is always less than n . In ionic crystals, $m \sim 1$ and $n \sim 12$. In molecular crystals, $m \sim 6$. Note that $m = 1$ corresponds to coulomb attraction between two point charges. At temperature T_1 , corresponding to energy E_1 , the interatomic distance oscillates from r_1^1 to r_1^{11} with a mean separation of $r_1 = (r_1^1 + r_1^{11})/2$. At a temperature $T_2 > T_1$, the energy is E_2 and the average interatomic separation is r_2 oscillating between r_2^1 and r_2^{11} . Note that $r_2 > r_1$ leading to thermal expansion. Thus, the asymmetric shape of the potential energy curve, which results in anharmonic nature of the lattice vibrations, is responsible for the thermal expansion. A large binding energy leads to a high melting point of a material, i.e., a deep potential energy minimum; in this case, at not too high temperatures, the potential energy curve would be asymmetric only to a small extent. Therefore, a material with a high melting point ($T_m^\circ \text{ K}$) would, near room temperature exhibit a low thermal expansion coefficient (α). The product (T_m), is often empirically found to be constant for a series of related materials.

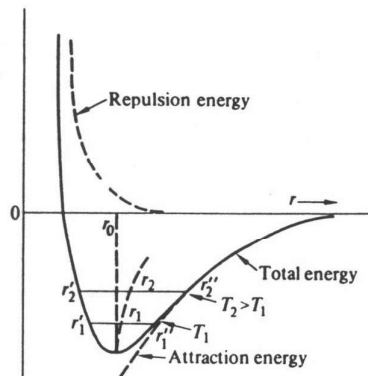


Fig 11.1 Potential energy Vs interatomic distance

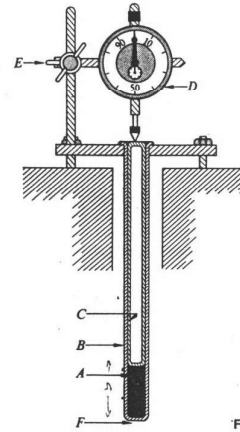


Fig. 11.2 Dilatometer assembly

Isotropic materials can be described by a single potential energy curve and therefore exhibit the same thermal expansion in all directions i.e. have a single value of α . However, non isotropic crystals have potential energy Vs r curves of different shapes in different directions; consequently they possess different α values in various directions. A poly crystalline specimen of randomly oriented non isotropic crystals exhibits an expansion behavior which is an average of that in the various directions. Similarly a multiphase material has thermal expansion behavior which is a weighted average of the expansion coefficients of its component phases. Differential dilatation in different directions in non isotropic materials or in different grains in a multiphase material, may lead to micro cracks and poor mechanical strength.

Determination of the thermal expansion coefficient requires the measurement of two physical quantities, displacement and temperature, for a sample of the material that is undergoing an appropriate thermal cycle. A diverse range of techniques can be employed for this purpose, and the main ones are outlined below.

i) Dial gauge (mechanical magnification) (ii) Optical lever (tilting mirror moves a light beam) (iii) Electrical transducer (capacitive or inductive) (iv) Resistance strain gauge (v) Optical interferometer. Of these the dilatometer with the dial gauge is the simplest and the most common method.

Mechanical Dilatometry is one of the most popular techniques for thermal expansion measurement. A specimen is heated in a furnace and the displacement of the ends mechanically transmitted to a displacement sensor by means of push rods. These can be made from low expansion fused silica for operation to 700°C. Alumina can extend the technique to 1600°C, and more extreme temperatures require the use of graphite. By compensating for the expansion of the push rods, accuracies of around 1-2 % for the CTE can be obtained.

Equipment:

A quartz tube, dial-gauge dilatometer, Furnace, Power supply, Temperature controller, Potentiometer, Thermocouple (chromel-alumel). Specimens (Pyrex. soda-lime-silica glass. aluminum. mild steel. building brick. fireclay brick. etc.

Procedure:

1. Mount one of the samples (A) at the bottom of the quartz tube (B) which is closed at one end. A quartz tube (C), closed at both ends, is placed on top of the specimen. A dial gauge (D), with a least count of 0.001 mm, is attached to the top of the outer quartz tube by an inconel clamp (E). The completed assembly is shown in Fig. 11.2
2. The whole assembly is inserted in a tube furnace, the temperature of which is controlled with a chromel-alumel thermocouple.
3. The apparatus is equilibrated at different temperatures. The dial gauge reading and the temperature of the specimen determined with a thermocouple (chromel-alumel) located at F (Fig11.2) and a potentiometer.

Observations:

1. Note the initial dimensions of the sample and the dial gauge reading.
2. Plot. (L/L_0) Vs Temperature.
3. Calculate the average linear thermal expansion coefficient from the plot.

$$= (1/L_0) . (L/T)$$

Questions

1. How do you correct the value of ?
2. What is the volume expansion coefficient of your sample?

3. Why are quartz and inconel used for dilatometer construction?
4. Why do we use a quartz tube closed at both ends instead of a quartz rod?
5. Can you use the same dilatometer for measurements below room temperature?
6. What is the magnification of the dial gauge that you used? How can you increase it?

Experiment 7

Recovery, Recrystallization and Grain Growth

Grain Size Measurement by Quantitative Metallography

Aim: To report microstructural changes in a cold worked single phase alloy during its annealing and grain size determination of recrystallized alloy by quantitative metallography

Theory:

A. Recovery, Recrystallization and Grain Growth:

Metals can be plastically deformed. i.e. they will not come back to their original shape and size when the load causing their deformation is removed. Thus, we can roll a metallic strip to reduce its thickness. Similarly, there are many other metal working operations which are industrially used to make components and parts of many engineering devices from metallic materials.

A small percentage of the energy spent in plastically deforming a metal remains stored in its structure and increases its internal energy. This increment in the internal energy is associated with the generation of lattice defects such as vacancies, interstitials, dislocations and stacking faults during plastic deformation of the crystal. On a microscopic scale the distribution of these defects, however is very inhomogeneous. For example, bulk of the deformed crystal consists of relatively dislocation-free regions (called sub-grains or cells) separated by boundary regions of high dislocation density in which many dislocations are arranged as tightly packed tangles. There may be many of such cells in each grain of the material. If the deformation occurs at a low enough temperature so that the crystal has very little thermal energy to recover from such a structure, dislocation tangles are retained in its structure and we refer to such a structure as the cold worked structure. What do you think will happen when such a structure is heated? Obviously, the crystal acquires thermal energy and with its help several thermally activated mechanisms, such as atomic diffusion begin to operate. Heating of a cold-worked (or cold-deformed) structure at a given temperature for a given period of

time is generally referred to as annealing. Phenomena which occur during annealing are recovery, recrystallization and grain growth.

Recovery

The first effect of reheating previously cold-worked metal is reduction of internal stress without noticeable change of mechanical properties. Since this effect is not evident microscopically, the importance of the recovery process has not been widely appreciated by engineers. Recovery in a cold-worked structure occurs when the material is held at relatively lower temperatures for a given time interval. It involves changes in the number and distribution of point defects and dislocations present in the cold-worked structure. Since the temperature of annealing is low during recovery, structural changes in the material occur by the clustering of point defects like vacancies and interstitials and the migration of point defects to dislocations, grain boundaries and/or external surfaces of the crystal. If the annealing is carried out at some what higher temperature even dislocations (which are less mobile than point defects) may gain appreciable mobility and move by *glide and climb* to relieve some of the internal strain accumulated in the structure. Some of the dislocations may rearrange themselves while some others may get annihilated by mutually canceling each other. Thus during the process of recovery of a cold-worked material the dislocation density of cells gets reduced and dislocation walls around these cells become more sharply defined. Small changes in hardness which are usually observed during later stages of recovery are due to decrease in the number of point defects and dislocations.

Recrystallization

Recrystallization entails the complete formation of new and unstrained metal grains, with simultaneous elimination of previously cold-worked and distorted metal. Recrystallization is very evident because of its marked effect on mechanical properties. Strain hardening and work strengthening which resulted from cold working are largely eliminated by recrystallization and ductility is simultaneously restored. The microscopical appearance of cold-worked metal is also greatly changed by recrystallization.

When annealing is carried out at even higher temperatures recrystallization occurs. During the recrystallization process new strain-free grains crystallize in the earlier cold-worked structure. The free energy of the system is lowered by these newly formed strain-free grains. In an aggregate of deformed metal crystals, there are regions where the atomic structure is most highly disarranged, and such regions exhibit the strongest tendency for realignment into an unstrained condition and the strongest desire for recrystallization. These regions are at grain boundaries, at slip planes or twinning planes, at internal discontinuities, regions of stress concentration caused by inclusions, and elsewhere with the crystal where internal strain is high. These new grains grow at the expense of the deformed structure until the whole matrix is consumed. This process occurs either by migration of original grain boundaries or by sub-grain growth. The recrystallized matrix has much lower dislocation density than the deformed material. The lowest temperature at which strain-free recrystallized grains appear in the structure of the previously cold-worked structure is termed as the recrystallization temperature of that material. The recrystallization temperature is influenced by the grain size, the severity of cold-work, strain given during plastic deformation, the presence of solute atoms and the second phase in the structure.

Greater prior cold working increases the number of recrystallization nuclei and ensures finer grain size after complete recrystallization. Greater plastic deformation also creates greater misalignment at grain boundaries and regions of internal strain, a factor which allows recrystallization at lower temperature. The recrystallization temperature is lower because less thermal agitation is necessary to obtain sufficient energy for the atoms to become rearranged by recrystallization.

Finer initial grain size results in more strained regions in plastically deformed metal, which in turn causes finer grain size in the fully recrystallized metal. Nucleation and growth of new unstrained crystals are time and temperature dependent. For a given amount of plastic deformation, the rate of nucleation and the growth rate of the newly formed grains are more rapid at higher temperatures.

Recrystallization occurs by the continual formation of new unstrained grains and their growth until all the strained metal is replaced by unstrained material. The recrystallization temperature is defined as the temperature at which recrystallization is

complete, but it is usually much more satisfactory to think in terms of the range of temperatures between the first appearance of a new grain and complete recrystallization. This is called the recrystallization temperature range

It is not possible to cite particular recrystallization temperatures, since recrystallization depends upon several variables. Increased plastic deformation allows recrystallization at a lower temperature, as plotted in Fig. 12-1. The time of annealing also has an effect. Increased time allows recrystallization at lower temperature.

(Fig.12-2). Coarse grained metal is not work-hardened as much by a given amount of deformation as is finer-grained metal and will not have as great an urge to recrystallize. Therefore the recrystallization temperature will be higher for coarse-grained metal

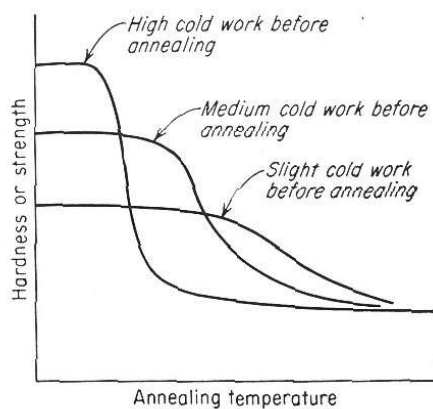


Fig 12.1 Effect of prior cold work on recrystallization temperature

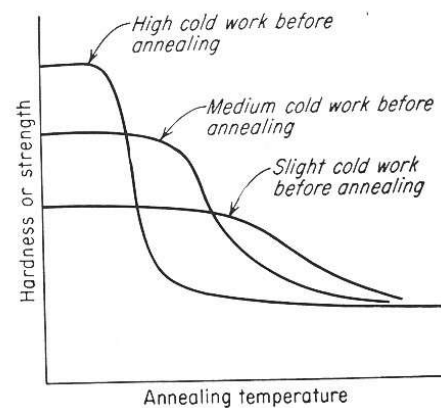


Fig 12.2 Effect of annealing time on recrystallization temp of cold worked metal

Grain Growth or Coalescence

When cold-worked metal is held above the recrystallization temperature after recrystallization is complete, growth of some of the recrystallized grains at the expense of other grains occurs, a process called grain growth or coalescence. This is a digestion process in which some grains increase in size while others get smaller and finally disappear, resulting in a larger average grain size and a smaller total number of grains. Grain growth occurs because in doing so the total area of grain boundaries reduces and lowers, in turn, the grain boundary energy of the system.

Because engineering properties of metals are related to grain size, control of grain growth is an important feature of the metallurgy of cold working and annealing. Control of grain size of cold-worked metal during heat treatment depends, to a large measure, upon control of prior history of the material, but a fine-grained structure can be coarsened by coalescence during annealing. Attempts to shorten the annealing time after cold working by utilizing a high furnace temperature may result in excessive coalescence. Overloading furnaces so that some parts of the charge are overheated before the entire charge is adequately softened may also result in excessive coalescence in the overheated portions.

Why do some crystals grow during coalescence while others become smaller and disappear? Grain-boundary migration is the fundamental feature that governs this condition, although the driving force for boundary migration is not completely known. When the boundary between two metal grains is perfectly plane, it has little tendency to migrate, and there is little tendency for one grain to digest its neighbor. However, boundaries that are not in plane appear to migrate toward the center curvature of the boundary. This tends to make large grains larger and small grains smaller until they disappear. Also, there may be a tendency for grains to grow in certain crystallographic directions preferentially to other directions.

A complete analysis of grain-boundary migration is not within the scope of engineering metallurgy, but this brief statement of possible mechanisms is included as a means of evaluating the effects of various working and heating cycles on boundary migration. Purer metals or alloys coalesce extensively, while less pure material retains fine grain size for longer annealing periods or at higher annealing temperatures. All metals, or even all heats of the same metal, do not develop similar grain sizes during forming and reheating processes, and do exhibit differences in subsequent operations and significant variation in final properties.

The Cold-work-Anneal Cycle

From the preceding discussion it is evident that cold working hardens and strengthens metals at the expense of decreased ductility. However, when cold working is excessive, the metal may fracture before reaching the desired size and shape. To avoid such defects, the total deformation is produced in several steps with intermediate anneals

to soften the hardened metal and to regain lost ductility so that further deformation is possible. This process of repeated cold working and annealing is called the cold-work-anneal cycle, which is illustrated for specific conditions in Fig. 13-20.

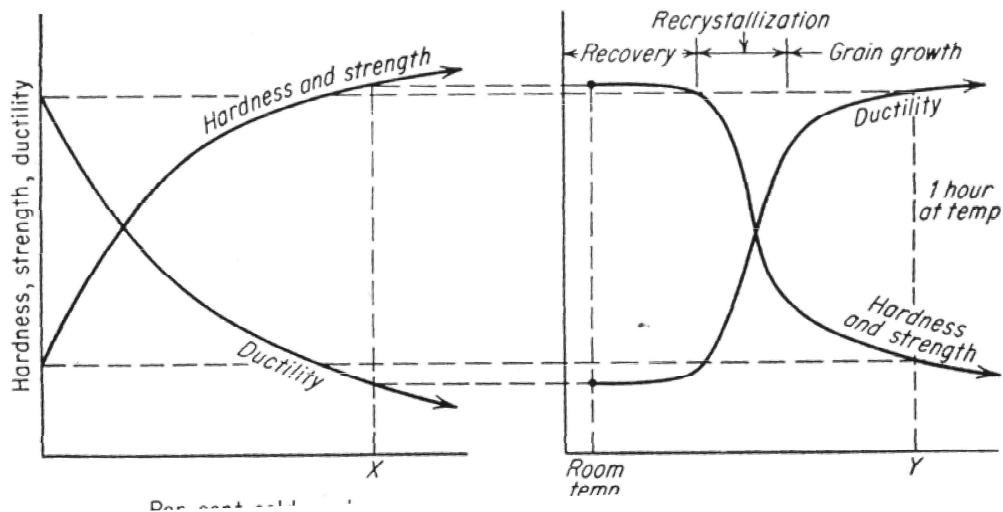


Fig 13-20. Cold-worked anneal cycle.

Metal is hardened and strengthened by cold deformation and ductility is decreased. Before the metal fractures, cold working is stopped as at X. If metal which has been previously deformed to point X is reheated for 1 hr at a temperature Y, the original ductility and strength will be returned. To obtain immediate properties the stock is annealed when sufficiently oversize so that the desired properties will be developed during a final working operation.

Metal is hardened and strengthened by cold deformation and ductility is decreased. Before the metal fractures, cold working is stopped as at X. If metal which has been previously deformed to point X is reheated for 1 hr at temperature Y, the original ductility and strength will be returned. To obtain intermediate properties, the stock is annealed when sufficiently oversize so that the desired properties will be developed during a final working operation. Consideration of these two operations, hardening and subsequent softening, as a unit is most important for engineering applications, since they allow a shape to be formed with any prescribed degree of work strengthening. When a completely softened product is desired, process annealing follows cold working. Complete recrystallization and softening result. However, if the final product must be

stronger than the fully softened material, it becomes necessary that the last recrystallization anneal precede final cold working, and then the softened metal must be

Grain growth occurs because in doing so the total area of grain boundaries reduces and lowers, in turn, the grain boundary energy of the system. In simple situations the occurrence of grain growth can be expressed in terms of the following relationship;

$$D_t^2 - D_0^2 = K t^n \quad (12.1)$$

Where D_t is the average grain diameter after the annealing time of t , D_0 is the initial grain diameter before grain growth starts, K and n are constants. Usually a value of n is estimated to be $1/2$.

Grain Size Measurement by Quantative Metallography:

From the study of actual grain shapes it has been found that while grains do not actually possess regular or idealized forms the truncated octahedron is a reasonable approximation for equiaxed grains. For the quantitative estimate of the average grain size of a single-phase equiaxed grain structure the grains along a line, circle or within a known area are counted. In Jeffries' Planimetric Method a circle surrounding a known area is superimposed on the microstructure as shown in Fig.12.4. The grains cut by the circumference, n_c and grains completely within the circle n_i are counted. Half of the number of grains intersected by the circumference is added to the number of completely included grains to get the number of equivalent whole grains within the circle. Thus

$$n_{eq} = \left(\frac{1}{2}\right).n_c + n_i \quad (12.2)$$

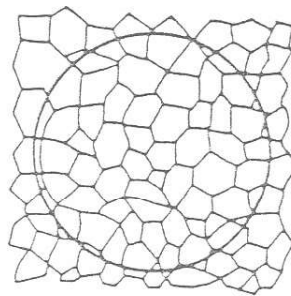


Fig 12.4 Grains size measurement by Jefferies Planimetric method

From the analysis of the distributions of sections in space, occupied by truncated octahedra, the ASTM (American Society of Testing Materials). System gives the following relationship

$$N_a = 2^{N-1} \quad (12.2)$$

where n is the number of grains per square inch at 100x and N = ASTM grain size index number. In the ASTM method the microstructure of a given single-phase polycrystalline specimen when observed at a magnification of 100X is compared with a set of standard photomicrographs.. The charts are indexed for N varying from 1 to 8.

Equipment:

Metallurgical microscope, A calibrated eyepiece and Six polished and etched specimen of a single phase material of cold rolled and annealed samples

Procedure:

1) Observe the microstructures of Sample No.1-6. Note the difference in the shape of grains in each cold rolled and recrystallized sample. Note the absence of any recrystallization activity in Sample No.2 and formation of a few recrystallized grains Sample No.4. Also observe the difference in the grain structure of Sample Nos.5 and 6

(2) Calculate the ASTM grain size for sample 6.

Report:

(1) Schematic diagram of micro structures of Sample Nos.1 - 6.

(2) Mention the etching reagent used.

Questions:

1. What factors are expected to raise the recrystallization temperature of a metal or alloy? Why?
 2. If we hold the cold worked sample in the furnace for a very very long time at a temperature above its recrystallization temperature {will the grain growth continue or will it stop at some stage? Explain.
 3. During recrystallization where do new grains will first form? Why?
 4. Why is metal able to plastically deform under a given load, while glass breaks?
-

Experiment No. 8

Strength reliability of brittle solids

Introduction

Our everyday experience of brittle materials (such as, glass, ceramics) tells us how easily these materials break under application of load – *window panes being broken by cricket balls in the hostels*. Deformation of brittle materials is characterized by rapid fracture and without plastic deformation. Measurements show large variability of mechanical properties of such materials (*in contrast ductile materials, such as structural steels, show marked reproducibility in their mechanical properties*). This large variability arises because of the presence of cracks or flaws. The cracks of various sizes and orientation are distributed in brittle materials. For example, figure 1 shows an image of a glass surface with cracks. The strength of the material is affected by the size and orientation of the cracks. Figure 2 shows two specimen under uniaxial tensile loading with in one case a surface crack and in another case an internal crack. In both cases the cracks are normal to the tensile axis.. And in both cases the fracture stress (for a brittle material) is given by the following equation (this equation is well known to researchers as the Griffith Equation¹):

$$\sigma_f = \left(\frac{2E\gamma}{\pi a} \right)^{1/2} \quad (1)$$

where, E is the Young's Modulus, γ is the surface energy, and a is the crack length (as defined in figure 2).

Equation (1) clearly shows that the fracture strength is sensitive to crack length and it reduces as the crack length increases. As a material can have wide distribution of crack sizes, different samples show large variation in strength. Of course, variability in strength can be dealt by taking an average value. However, the engineer must realize that some components would fracture much below this average value. One of the aims of this lab is to show the dispersion in strength and also to establish methods for characterization of the strength of brittle materials.

¹ “Mechanical Metallurgy” by G.E. Deiter. See section 7.4 (Chapter 7) on “Griffith Theory of Brittle Materials”.

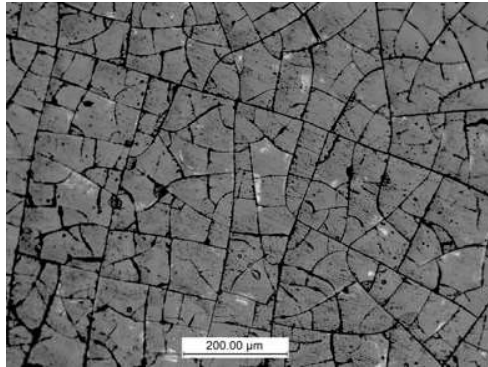


Figure 1: An image of cracks on a glass surface.

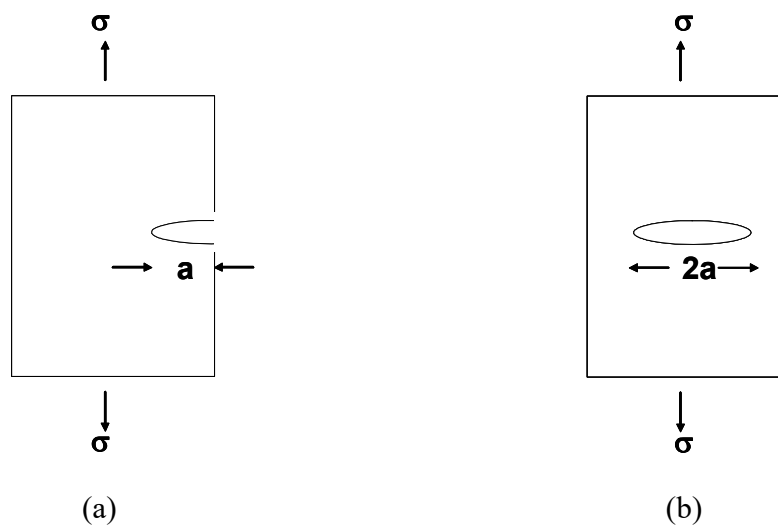


Figure 2: Uniaxial tensile loading of a brittle material in the presence of crack: (a) surface crack of length a , and (b) internal crack of length $2a$.

Toughening of Brittle Materials

If cracks or flaws could be eliminated (or considerably reduced) then brittle materials would show much higher fracture stresses and lower variability in their strengths. Examination of figure 3 and equation 1 reveals that surface cracks have a much more effect than the internal cracks on the deterioration of strength. A simple method of eliminating the surface cracks is to remove the surface layer. This, in case of a brittle material like glass, can be easily achieved by treating the glass surface by a HF solution (concentration can be kept as low as 5%) for about 10 to 15 minutes. This will ensure removal of surface layer and exposure of a relatively crack free surface.

Alternatively, toughening² can also be achieved by introducing compressive stresses on the surface. The compressive stresses on the surface would prevent cracks from growing, thereby improving the strength. Compressive stresses could be introduced on the surface by thermal or

² “Fracture Phenomena and Strength Properties of Chemically and Physically Strengthened Glass”, A.L. Zulstra and A.J. Burggraaf.

chemical treatment. For example, glass can be toughened by heating to a high temperature (about 600°C) followed by quenching. This sets up compressive stresses on the surface. An alternative method involves dipping the glass in a molten salt. In the case of glass (which contains Na^+ ions), the smaller Na^+ ions can be replaced by the larger K^+ ions. This can be achieved by dipping such a glass in molten KNO_3 for about 10-15 minutes. The ion exchange by the larger ions leads to a compressive stresses on the surface. Conversely, if the Na^+ ions are replaced by smaller Li^+ ions (as would be the case if the glass is dipped in molten LiNO_3) then tensile stresses would be set up on the surface. This would lead to a deterioration of the properties of glass, as the tensile stresses would result in the growing of surface cracks. The surface cracks, shown in glass (see figure 1), were made visible by treating the glass with molten LiNO_3 (*normally the cracks are too small to be easily visible*). Knowing an average strength (fracture stress) of a brittle material, equation (1) can be used make an order of magnitude estimate of the crack size. For this estimate you will need to know the Young's modulus and the surface energy. For a glass slide these values could be taken as: $E = 70 \text{ GPa}$; $\gamma = 0.2 \text{ J/m}^2$.

Another aim (other than the one mentioned in the previous section) of this lab is study the toughening techniques and their effect on the variability of strength in a brittle material like glass.

Bend Testing for Brittle Materials

The uniaxial tensile test (introduced in the tensile testing lab). a straightforward technique for measuring the fracture strength of materials, works very well for ductile materials. However, in case of tensile samples made from brittle materials, very often the sample breaks near the grips leading to erroneous results. Therefore, bend testing is the usual method for evaluating strength of brittle materials. Two types of bend testing arrangements are shown in figure 3. The specimen is in the form of smooth rectangular plate, as is shown in this figure.

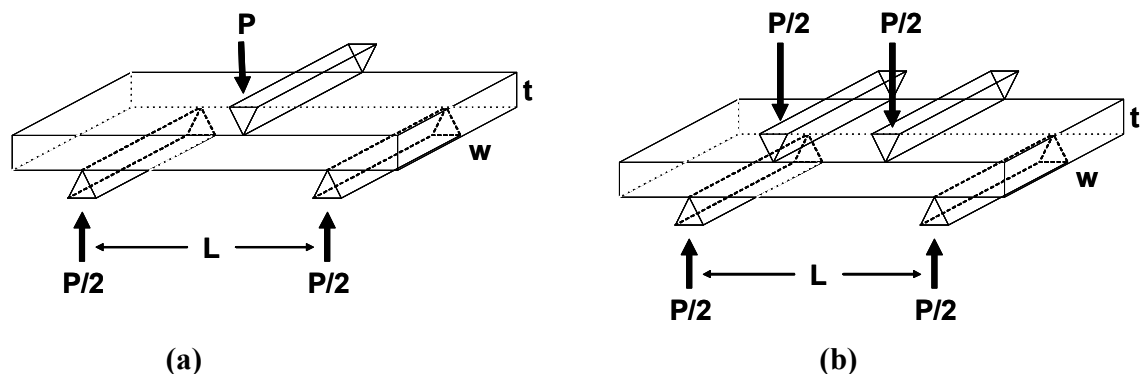


Figure 3: Bend testing of a rectangular plate: (a) three-point loading and (b) four-point loading

Here we will focus on the three-point bend testing arrangement (figure 2a). The same equipment that is used in tensile testing is used for the three bend test. However, a different jig for gripping the rectangular plate specimen is used, as shown in figure 4.

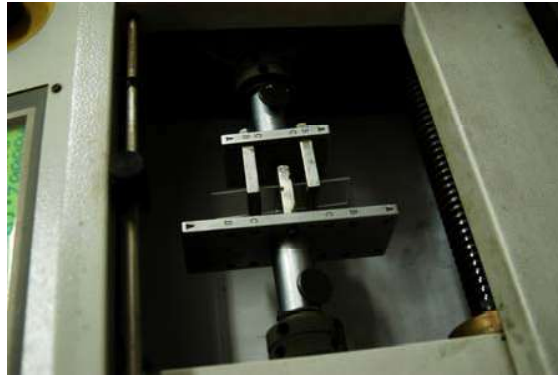


Figure 4: Rectangular plate (glass slide) is gripped in a special jig to produce three-point loading configuration, shown in figure 3(a).

Stress distribution in the plate, under three-point bending, is shown in figure 5 (*students who have done a course on “Mechanics of solids”, would be familiar with this diagram*). The bottom half of the plate is under tension, while the top half is under compression. The maximum tensile stress is at the middle of the plate and is given by the following expression³:

$$\sigma = \frac{PL}{wt^2} \quad (2)$$

where, P is the load, and L, w and t are the dimensions defined in figure 3(a).

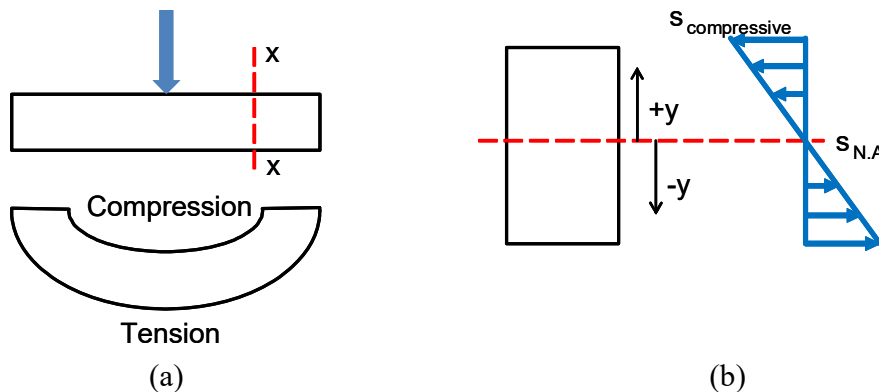


Figure 5: Under three-point bending: (a) Upper part of the plate is under compression, while the lower part of the plate is under tension. (b) The distribution of compressive and tensile stresses.

In a bending test, as the displacement increases continuously the load increases leading to a continuous increase in the stress (as per equation 2). Thus, fracture stress (or the strength of the specimen) is the stress at which the specimen fractures. Figure 6 shows a sample load displacement curve for bend test of a brittle material. As discussed earlier, in case of brittle materials, one would find a wide variation of strength even though the test is conducted under identical conditions. It is this variability that we now need to characterize.

³ “Mechanics of Solids”

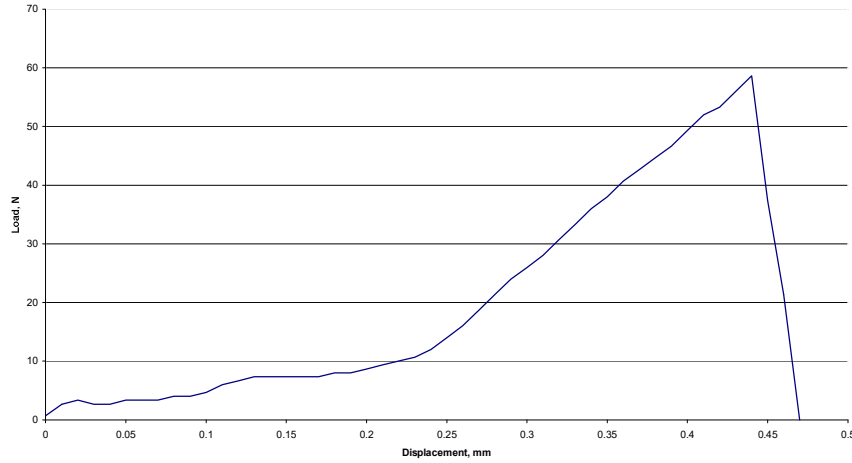


Figure 6: A load-displacement curve obtained in a three-point bend test for a brittle material.
Characterization of Variability of Strength in Brittle Materials: Weibull Distribution

Since there are random effects (due to random distribution of cracks) involved, the variability of strength will have to be dealt in a statistical manner⁴. One simple procedure for characterizing the variability of strength is by experimentally estimating the mean and standard deviation. This could be done by testing about 15-20 specimens. The mean strength and its standard deviation makes sense only if the distribution of strength follows a normal curve. It is found that in cases of wide variability (which is often the case for brittle materials) strength does not follow the normal curve.

A very commonly used method is to characterize the strength of brittle materials by assuming the so called “Weibull Distribution”. The probability of failure, P_S (*not to be confused with the load P in equation 2*) at stresses below σ_f , is given by a simplified version of the Weibull distribution function:

$$P_S = 1 - \exp \left\{ - \left(\frac{\sigma_f}{\sigma_o} \right)^m \right\} \quad (3)$$

where, m is the Weibull modulus, and σ_o is a characteristic strength of the material. The significance of the Weibull modulus, m , can be understood in terms of its relationship to the scatter of fracture strength about a mean value. A small value of the modulus signifies a large scatter (as would be the case for brittle materials). Whereas, for ductile materials the Weibull modulus is large, implying a small scatter. For ductile materials like metals, the Weibull modulus is about 50.

Equation (3) can be linearized as follows:

$$\ln \left\{ \ln \left(\frac{1}{1 - P_S} \right) \right\} = -m \ln(\sigma_o) + m \ln(\sigma_f) \quad (4)$$

⁴ “Mechanical Metallurgy”, G.E. Dieter. See Chapter 16 on “Statistics Applied to Mechanical Testing”.

Equation (4) is a linear equation of the form:

$$y = A + Bx \quad (5)$$

where, $y = \ln\left\{\ln\left(\frac{1}{1-P_s}\right)\right\}$, $A = -m \ln(\sigma_o)$, $B = m$, and $x = \ln(\sigma_f)$.

In order to determine the Weibull parameters, several tests (typically 10-15) would need to be done. In each test, the breaking load (i.e., peak load in figure 6) would have to be noted and the corresponding strength, σ_f , calculated from equation (2). Now, rank the strength data, i.e., sort the strength data in ascending order. Thus, suppose we have a data set of n values, the smallest strength value will have a rank of 1, second smallest rank of 2, ... and the largest strength value will have a rank of n . Now, the probability of failure, P_s , at stress level corresponding to rank i is given by:

$$P_s = \frac{i}{n+1} \quad (6)$$

The Weibull modulus, m , can be determined by doing a best fit of equation (5) to the experimental data using the linear least squares technique. Following equations (which give the best fit) can be used to determine the coefficients A and B of equation (5):

$$\bar{y} = A + B\bar{x} \quad (7a)$$

and

$$B = \frac{S_{xy}}{S_x^2} \quad (7b)$$

where, \bar{x} and \bar{y} are average values, and $S_{xy} = \frac{1}{n} \sum (x - \bar{x})(y - \bar{y})$ and $S_x^2 = \frac{1}{n} \sum (x - \bar{x})^2$.

Equation (7a) simply states that the best fit line passes through the point (\bar{x}, \bar{y}) . The interested student can find more details of the least squares method for obtaining the best fit.

Design of Experiment

The overall aims of this laboratory are to bring out the variability of strength and to understand the toughening techniques for brittle material. The material being given to you are glass slides (whose typical composition would be: Na_2O , CaO and SiO_2).

Following questions should help you design the experiment:

1. What equipment you would be using in this laboratory?
2. What toughening techniques you could employ for the glass slides?
3. Which specimen dimensions are required?

4. What experimental quantity you would measure to calculate fracture stress?
5. How would you compare the strength of the glass slides in the untreated condition and after application of toughening techniques?
6. How many samples you need to employ?

Before proceeding with the actual experiments, discuss your answers to the above questions with a lab personnel. Use the points given below to help you write a suitable lab report.

1. State the specific objectives of the experiment.
2. Create appropriate tables (with pertinent column headings) to tabulate the experimental data. The tables should also have columns in which you can tabulate the calculated results.
3. The report should clearly exhibit the variability of strength of glass slides and the effect of toughening treatment on this variability.
4. Based on your experimental results, make an order of magnitude estimate of crack sizes in the glass slide.

In this experiment, it is expected that you would use a spreadsheet program (such as, Microsoft Excel) for tabulating the data, performing linear least squares and producing the Weibull plots.

Experiment 9

Conductivity of Ionic solids and Ceramic Sample

Aim:

- a. To report resistivity variation of NaCl with temperature and report vacancy migration energy E_m and the energy of formation of vacancy pairs E_f .
- b. To measure room temperature resistivity of Zirconia sample and report resistivity variation with temperature.

Theory:

1. Introduction

Atoms in a solid are bound to the neighbouring atoms and occupy fixed positions relative to each other in what we call a crystal lattice. If this were entirely true, then have you ever wondered how does current flow in solids (forget about the metals!) or how do atoms of one metal mix into those of the other when we make a junction between them or how do they conduct heat. The answer to all these queries is simple. The solid state is far from static. Thermal energy keeps the atoms vibrating vigorously about their lattice positions and continually bumping into each other and exchanging energy with their neighbors and surroundings. Every now and then, an atom will gain sufficient energy to leave its lattice site and migrate. This motion is termed diffusion and a prerequisite for diffusion and electrical conductivity is the presence of point and electronic defects.

In many ceramics, diffusion and electrical conductivity are inextricably linked for two reasons. The first is that *ionic species* can be induced to migrate under the influence of a chemical potential gradient (diffusion) or an electric potential gradient (electrical conductivity). In either case, the basic atomic mechanism is the same. It is the presence of point defects which makes both these processes possible. The defects are always present and provide a thermodynamically stable state for the solid. These defects can be in the form of vacancies, interstitial atoms or impurity atoms. Schottky defect is the most common form of defect in ionic solids such as NaCl. The defect concentration is dependent on temperature and type of impurity present. At a given temperature, the concentration of pair of positive ion and negative ion vacancies is given by:

$$n = C \cdot \exp(-\phi/2kT) \quad \dots\dots\dots (9.1)$$

where,

C is a constant

ϕ is the energy of formation of such a pair

k is Boltzmann constant

T is the temperature in Kelvin

The positive ions surrounding a positive ion vacancy will have a finite probability of jumping into it. As a result, the vacancy will move through the crystal by virtue of positive ions jumping into it and diffusion (i.e. ion movement without any external field applied) becomes possible. When an electrical field is applied to the solid, the probabilities of ion jumps in the direction parallel and antiparallel with the field are altered so that there is an effective movement of positive ion vacancies toward the anode. This means that there is a net effective movement of positive charge toward the cathode. The expression of conductivity, σ , derived on this basis is of the following form:

$$\sigma = A \exp \left(- \left(\frac{E_m + \frac{\phi}{2}}{kT} \right) \right) \dots\dots\dots (9.2)$$

where,

A is a constant

E_m is the activation energy for migration

ϕ is the formation energy of vacancy pairs

k is the Boltzmann constant

T is the temperature in Kelvin

2. Resistivity variation of NaCl

The electrical conductivity of alkali halides such as NaCl is mostly due to the presence of point defects e.g. Schottky and Frenkel defects. The conductivity of NaCl increases as the temperature is increased partially due to increase in number of defects and partially due to their enhanced mobilities at high temperatures. There is a discontinuity observed in the conductivity somewhere within the temperature range of 400-700°C. The temperature corresponding to this discontinuity is called break point and this is known to arise from the presence of divalent impurities in the crystal. Each divalent impurity must create a positive ion vacancy to conserve charge neutrality. Thus at lower temperatures, such crystals possess more number of positive ion vacancies than predicted from thermodynamic considerations alone. In fact, below a critical temperature, all the vacancies are due to divalent impurities present. Thus the temperature dependence of conductivity is determined by mobility energy, E_m upto a critical temperature. Above this temperature, thermally generated vacancies dominate over the vacancies due to impurity and the overall temperature dependence of conductivity is given by the sum of mobility energy and energy of formation of vacancies, $E_m + \Phi/2$.

The arrangement for resistivity variation and vacancy formation in NaCl is shown in the Figure 9.1 overleaf.

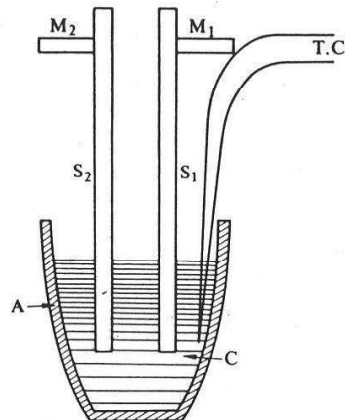


Figure 9.1

Here, A is alumina crucible, C is polycrystalline sodium chloride, S_1 and S_2 are two mild steel plates for electrical connectivity and also act as electrodes. T.C. represents the chromel-alumel thermocouple wires.

3. Kroger-Vink notation:

In a pure binary compound, the following defects exist:

1. *Vacancies*
2. *Interstitial atoms*
3. *Misplaced atoms*
4. *Free electrons*
5. *Electron holes*
6. *Interstitial and substitutional impurities*

A universally adopted scheme to denote these defects is the Kroger-Vink notation. In this notation, the defect is represented by a main symbol followed by a superscript and a subscript.

Main symbol: The main symbol is either the species involved, i.e., chemical symbol of an element, or the letter **V** for vacancy.

Subscript: The subscript is either the crystallographic position occupied by the species involved or the letter *i* for interstitial.

Superscript: The superscript denotes the effective electric charge on the defect, defined as the difference between the real charge of the defect species and that of the species that would have occupied that site in a perfect crystal. The superscript is a prime (') for each negative charge, a dot (•) for every positive charge, or an x for zero effective charge.

For example consider NaCl:

Na at Na site is represented as $\text{Na}_{\text{Na}}^{\times}$,

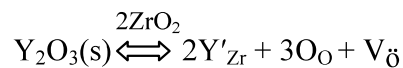
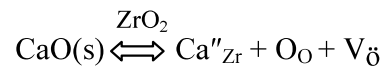
a vacancy at Na site is represented as V_{Na}' ,

Likewise, Cl at Cl site is represented as $\text{Cl}_{\text{Cl}}^{\times}$ and

a vacancy at Cl site as $\text{V}_{\text{Cl}}^{\bullet}$

4. Resistivity variation of Zirconia

Zirconia is a very important ceramic having wide applications as refractory material, insulator, abrasive, enamel, jewellery, electroceramic, sensors etc. It has very high melting point e.g. 2715°C, low thermal conductivity, high fracture toughness, high hardness, high wear resistance and it is chemically very inert. The electrical conductivity in Zirconia is predominantly a ionic conduction process that occurs above 600°C. However, at lower temperatures, n-type conduction process has been reported to explain the conductivity of Zirconia. Zirconia is usually used as calcia-stabilized zirconia or yttria-stabilized zirconia. The addition of either calcia or yttria to it results in defects represented by following equations respectively:



The excess electrons may not remain localized at the vacant site (V_{O}) and become separated giving rise to electronic conduction represented as

$$\text{V}_{\text{O}} = \text{V}_{\text{O}} + \text{e}''$$

The two probe method can be used to study the conductivity variation of Zirconia

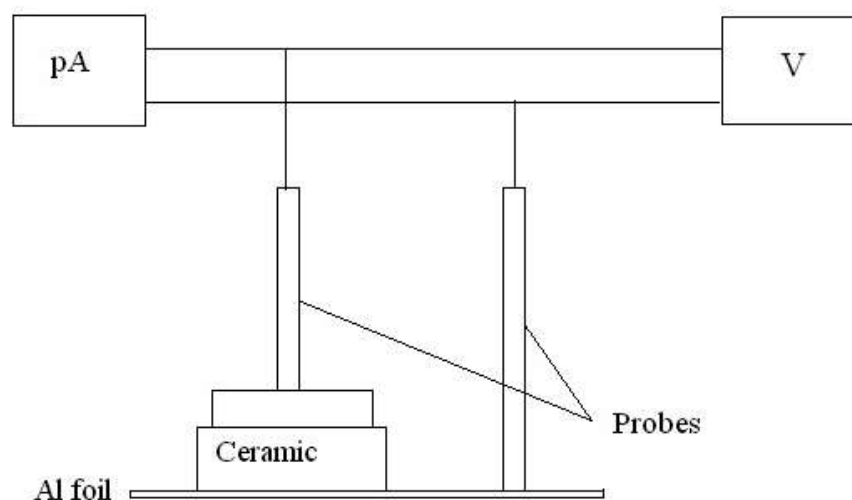


Figure 9.2: A schematic of the two probes set up

The arrangement for conductivity variation of ceramic sample is shown in Figure 9.2 Here pA is the picoammeter, V is voltage supply .

5. Design of the experiment:

Now since you know the basic mechanisms responsible for the conduction in ionic solids, you need to design an experiment to achieve the aims of the experiment with following perspectives:

1. What equipments would you be using?
2. What parameters would you be measuring and what will be the parameter that is to be varied?
3. What temperature domains you would be working in and how do you determine these?
4. What would be appropriate intervals at which you will need to take readings?
(Mind you, you have only three hours to design, perform and produce the results of experiment)
5. How would you analyze the results obtained from the experiments? Hint: graphs

Before you start performing the experiment, discuss the answers to above questions with the lab TA. Following points would be helpful in writing a suitable lab report.

1. Clearly specify the objectives of the experiment.
2. Note down the equipment you would require.
3. Make tables with appropriate column heads and note down the experimental readings.
4. Create appropriate plots to determine the experimental quantities you aim to find.
5. Write your results and compare with the values reported in literature. If there is any discrepancy, discuss the possible causes.

Questions:

1. From your data determine E_m and Φ (in eV)
2. As you know that vacancy formation takes place at higher temperature than migration of vacancies. You may get two different slopes on the graph corresponding to the two processes. Determine the point (break point) at which you obtain discontinuity in slope.
3. Why is it important to use a.c. for this experiment (NaCl)?
4. If some CaCl_2 powder were added to NaCl, which way the breakpoint moves? Also write the defect equations using Kroger-Vink notation.
5. What is the limitation of two point probe method and why it is useful for high resistivity samples such as ceramics and not semiconductors? What you can do to overcome the limitations of two probe method? What is the reason for exceptionally high resistivity of ceramics?

EXPERIMENT -10

Electric Characterization of Semiconductors

Aim:

- (a) Room temperature measurement of resistivity, carrier concentration and carrier mobility for a semiconductor having a majority carrier, either n- or p- type (using Hall measurement set-up)**
- (b) Temperature dependent measurements of resistivity to evaluate band gap energy (E_g) in germanium (Ge) semiconductor (using Four-point probe set-up with furnace)**

1 Theory:

1.1 Electronic structure of materials

Solids are classified into three main groups namely metals, insulators, and semiconductors, on the basis of their energy bands. Energy bands of any solid are obtained from solution of Schrödinger's equation for that solid, and represent the electron eigen energies as a function of the electron wave vector [i.e. momentum]. The results of a hypothetical quantum-mechanical calculation of electron energy as a function of the lattice spacing for silicon as shown in Fig 1.1 This schematic is very instructive for qualitative understanding of the occurrence of energy bands and forbidden energy gaps. A solid can be approximated to an ideal gas wherein each isolated atom has its discrete electron energy levels [two levels are shown on the far right of the diagram]. These Eigen energies expand into energy bands, as we decrease the inter-atomic spacing to form a solid. As the inter-atomic spacing is reduced, the interaction between atoms takes place and keeps increasing. Finally, in a solid, atoms very strongly interact with each other, and the valence (the outermost) electrons cannot claim to belong to any particular atom. What this means is that if the solid has N atoms, each atomic level must split (to remove degeneracy) into N sub-levels, very closely spaced to each other [as N is a very large number] to accommodate electron levels of N atoms. This is how an energy band of very closely spaced sub-levels evolves. The energy gap between the allowed energy bands is the forbidden energy gap or band gap E_g . In the quantum mechanical picture,

electrons cannot have any energy in the forbidden energy range. The highest completely filled [i.e. occupied with electrons] energy band at 0K is called valence band, and the next higher band is called the conduction band. Fig.1.2 illustrates the basic differences between the 3 classes of solids in terms of the valence and conduction bands. In Fig.1.2, the abscissa is some x-direction in the solid, while the ordinate is the electron energy. As Fig.1.2(c) indicates, the metals are characterized by overlapping conduction and valence bands or partially filled conduction bands. The shaded area represents energy levels occupied by electrons. The non-metals, i.e. semiconductors and insulators, are characterized by completely empty conduction bands at 0K. Semiconductors have smaller band gap than insulators, as indicated in Figs. 1.2(a) and 1.2(b).

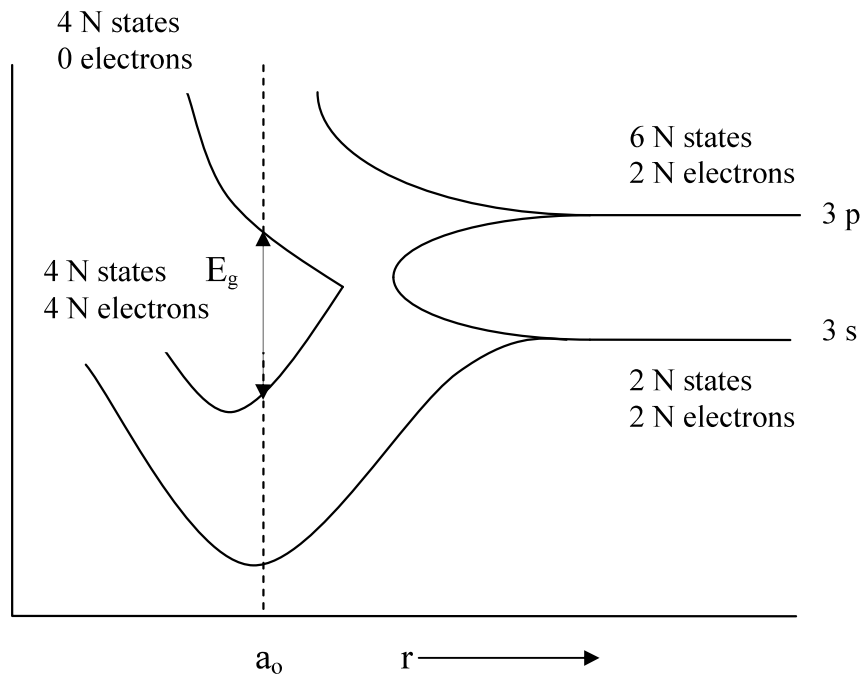


Fig 1.1 The splitting of 3s and 3p energy levels in silicon to form allowed and forbidden bands

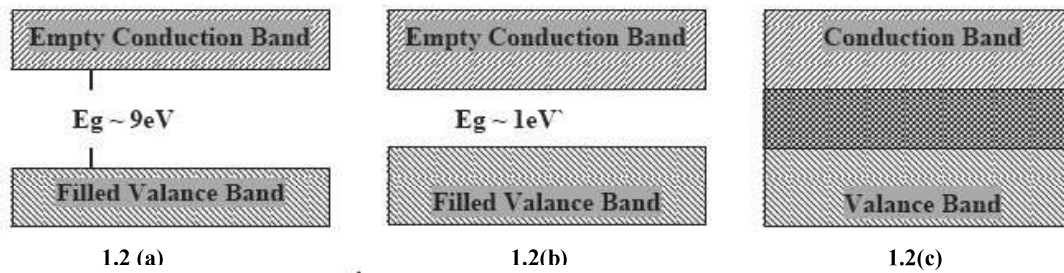


Fig 1.2 Schematic energy band representation of
a) Insulator b) Semiconductor c) Metal

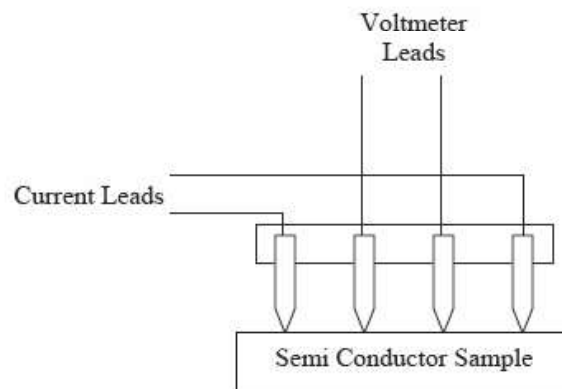


Fig. 1.3 Four probe set up

In order to choose a material suitable for a particular device we need to know its electrical properties. In this experiment we will measure **resistivity, carrier concentration, carrier mobility, and band-gap of the semiconductor.**

1.2 Electrical Properties of materials

1.2.1 Resistivity measurement:

When an electron or a hole [i.e. a missing electron] responds to an applied electric field it accelerates, and gains kinetic energy. [A force acts on a charge carrier in an electric field.] This means that it is excited to a higher energy state. So, only those electrons and holes can respond to an applied electric field that has empty higher states available for excitation. [Note that Pauli's exclusion principle requires that no two electrons can have the same eigen energy, that too, only if they have opposite spins.] In a moderate electric field, gain in the kinetic energy is a very small fraction of the band gap energy. For this reason, the valence electrons in a non-metal at 0K cannot respond to an applied electric, as they see no higher states to which they can be excited. For this reason, a non-metal is a perfect insulator at 0K, as it has no conduction electrons or free carriers. [A free carrier is

free to respond to an applied electric field.] At room temperature [i.e. 300K], thermal vibrations break a minute fraction of the covalent bonds in a semiconductor. In other words, the thermal energy kT excites a very small fraction of valence electrons in a semiconductor over the band gap E_g into the conduction band. This fraction naturally depends upon the values of E_g and kT . This is known as thermal generation of free carriers. So thermal generation always gives rise to electron-hole pairs, i.e. equal numbers of conduction electrons and holes are created. The number of such pairs per unit volume is known as the intrinsic carrier density n_i which is given by:

$$n_i = C \exp\left(-\frac{E_g}{2kT}\right) \quad 1.2.1.a$$

C is a constant and has same unit as n_i , i.e. cm^{-3} , k is Boltzmann's constant, and T is absolute temperature. From equation [1.2.1.a], it follows that for a semiconductor at 300K, the conduction band is slightly filled with electrons, and the valence band is slightly empty for electrons, or slightly filled with holes. A conduction electron is a free carrier because it has empty higher states to which it can be excited to by gain in kinetic energy. A hole [which is always in the valence band] is also a free carrier, as it can be excited to all states filled by electrons. Note that in the energy band diagram, going up increases the electron potential energy, $-qV$, but decreases the hole potential energy, qV , where V is the electrostatic potential. When a conduction electron has no kinetic energy, then it is at the conduction band lower edge E_c . Similarly, when a hole has no kinetic energy, then it is at the valence band upper edge E_v . The free carrier density in the pure semiconductor is n_i . The conductivity of an intrinsic (pure) semiconductor is therefore proportional to n_i , while the resistivity, ρ , will be inversely proportional to it.

$$\sigma = n_i q(\mu_n + \mu_p) \quad 1.2.1.b$$

where q , μ_n and μ_p are electron charge, electron and hole mobility, respectively.

Four Point Probe Resistivity Measurement

The resistivity of a solid is obtained experimentally by passing a current through the solid, and measuring the current through and the voltage drop across the solid. This measurement is easier for metal. But for non-metal, the contact between metal current lead and non-metal sample act as high resistance junction. A metal semiconductor contact is a Schottky barrier diode. This a complication, because if the voltage is measured between the two current leads, then this will not only include the voltage drop

across the semiconductor, but also the large voltage drop across the two metal semiconductor contacts. For this reason the semiconductor resistivity measurements involves four equidistant probes, as shown in Fig 1.3. The two outer probes carry the current from a constant current generator, while the two inner probes are used for voltage measurement by a very high input resistance, then, there is no current flowing through the voltmeter. Ideally, the voltmeter should have infinite resistance then there is no current flowing through the voltmeter, hence there will be no voltage drop across the metal-semiconductor contacts at the voltage probes. This will ensure correct measurement of the voltage drop in the semiconductor in the region between the two inner probes. Note the current enters/leaves the semiconductor at the probes flowing vertically, while in the central region the two outer probes, it flows horizontally. Also, the current flux density is not uniform. These complications result in the following relation between the resistivity ρ , the probes spacing d , the current I , and the voltage V between the two inner probes.

$$\rho = 2\pi (dV/I) \text{ (correction factor)} \quad 1.2.1.c$$

Correction factor is based on the sample configuration and dimensions. For details see Appendix A.

1.2.2. Carrier concentration and mobility measurement

The resistivity measurements of semiconductors can not reveal whether one or two types of carriers are present; nor distinguish between them. However, this information can be obtained from Hall Coefficient measurements, discovered in 1879 by J. Edwin Hall.

Hall Effect measurement

Since current in a semiconductor consists of the movement of electrons or holes, or both, moving charges will respond to magnetic field that is not parallel to their motion due to Lorentz force. Now consider a bar semiconductor, having dimensions x , y , and z . Let J is directed along x and H along z then E_h will be along y , as shown in Fig 4.4. When there is no electric field, the charges follow an approximately straight line. However, when a perpendicular magnetic field is applied, electron and holes will be separated by opposite forces. They will in turn produce an electric field (E_H) which depends on the cross product of magnetic field, H and the current density, J .

$$E_H = R_H \cdot J \times H$$

1.2.2.a

where, R_H is called the Hall coefficient.

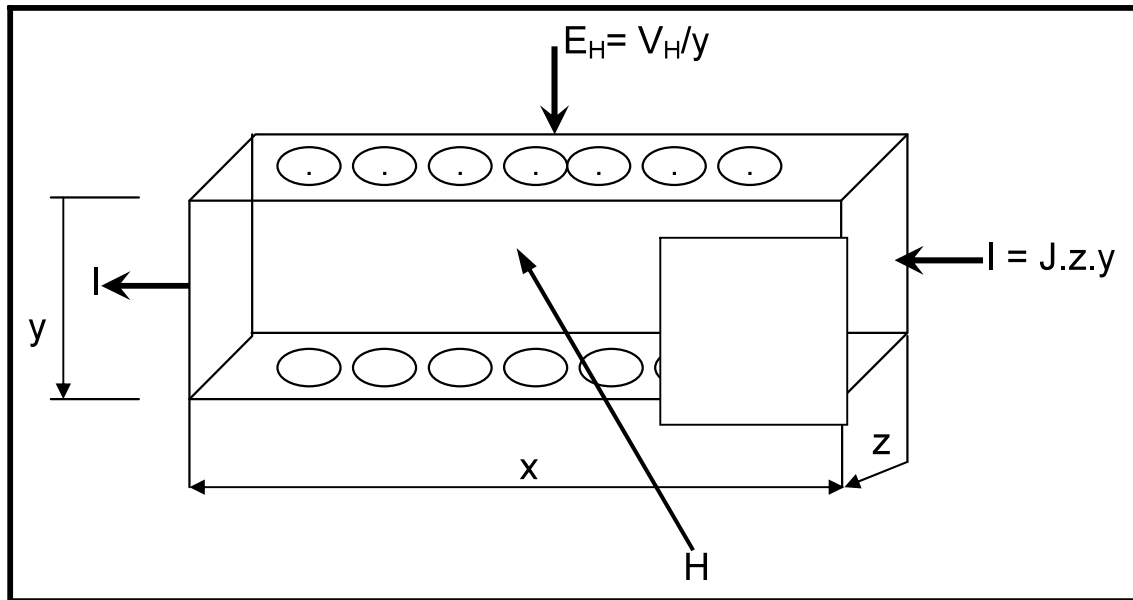


Fig. 4.4: Schematic of Hall coefficient measurement

Then we can write,

$$R_H = \frac{(V_H \cdot Z)}{IH} \quad 1.2.2.b$$

where, V_H is the Hall voltage appearing between the two surfaces perpendicular to y and

$$I = J \cdot y \cdot z \quad 1.2.2. c$$

In general, the Hall voltage is not a linear function of magnetic field applied; i.e the Hall coefficient is not generally a constant, but a function of the applied magnetic field.

However, it is easy to calculate Hall voltage if it is assumed that all carriers have the same drift velocity. We will do this in two steps.

(a) By assuming that carriers of only one type present

Metals and doped semiconductor are the examples of this type where one carrier dominates.

The magnetic force on the carriers is $F_m = e(v \times H)$ and is compensated by the Hall field $F_H = e E_H$, where v is the drift velocity of the carriers. Assuming the direction of various vectors as before

$$v \times H = E_H \quad 1.2.2.d$$

From simple reasoning, the current density J is the charge q multiplied by the number of carriers traversing unit area in unit time, which is equivalent to the carrier density multiplied by drift velocity i.e. $J = q n v$

By putting these values in equation (2)

$$R_H = \frac{E_H}{IH} = \frac{vH}{nqvH} = \frac{1}{nq} \quad 1.2.2.e$$

From this equation it is clear that the sign of hall coefficient depend upon the sign of the q . This means, in a p-type specimen the R_H would be positive, while in n-type it would be negative. Also for a fixed magnetic field and input current, the hall voltage is proportional to $1/n$ or its resistivity. When one carrier dominates, the conductivity of the material is

$$\sigma = n q \mu \quad 1.2.2.f$$

where μ is the mobility of the charge carriers.

Thus $\mu = R_H \sigma$, R_H is expressed in $\text{cm}^3 \text{ coulomb}^{-1}$ thus μ is expressed in units of $\text{cm}^2 \text{ volt}^{-1} \text{ sec}^{-1}$.

(b) By assuming that of both types carriers present.

Intrinsic and lightly doped semiconductors are the examples of this type. In such cases the quantitative interpretation of hall coefficient is more difficult since both types of carriers contribute to Hall field. It is also clear that for the same electric field, the Hall voltage of p-carriers will be opposite sign from the n- carriers. As a result, both mobilities enter into any calculation of Hall coefficient and a weighted average is result i.e

$$R_H = \frac{\mu_h^2 p - \mu_n^2 n}{2(\mu_h p + \mu_n)^2} \quad 1.2.2.g$$

Where μ_h and μ_n are the mobilities of holes and electrons, p and n are the carrier densities of holes and electrons. Eq. 1.2.2.g correctly reduces to equation 1.2.2.e when only one type of carrier is present.

Since the mobilities μ_h and μ_n are not constants but function of temperature (T) the hall coefficient give by Eq. 1.2.2.e is also a function of T and it may become zero, even change sign. In general $\mu_n > \mu_h$ so that inversion may happen only if $p > n$, thus Hall coefficient inversion is characteristics only of p-type semiconductors.

1.2.3 Temperature dependent measurement (band gap measurement)

The resistivity, ρ , is given by

$$\rho = C \exp\left(-\frac{E_g}{2kT}\right) \quad 1.2.3.a$$

where, C is a constant. A plot of $\ln(\rho)$ versus $1/T$ will therefore be a straight line, whose slope will be $E_g/2k$. Hence the band gap of a semiconductor can be determined from measurement of resistivity ρ as a function of temperature T .

Temperature dependent measurement

The semiconductor sample is in the form of wafer. The four-probe set is spring-loaded, with collinear and equally spaced probes, and Zn-coated probe tips. The set is mounted on a stand, current and voltage leads are provided [see Fig 4.3]. The probe set and the sample stage are arranged in a small box-type oven. The oven temperature can be varied from 300 to 475 K.

2. Design of experiment

In the interest of time, you are given two semiconductor samples that are already mounted in the Hall measurement and Four-point-probe set-up:

A. Resistivity, carrier type, carrier concentration and mobility

1. What parameters you need to measure resistivity, carrier type, carrier concentration and mobility?
2. What are the possible assumptions in each measurement?
3. Can you validate your assumptions via experimental data? What additional data you need to take in order to validate your assumptions?

(Answers are hidden in the text of the theory. So read it carefully)

B. Temperature dependent resistivity measurement

1. Measure the resistivity at room temperature.
2. What should be the heating rate of oven? Keep in mind you need to have enough time at a given temperature to take a reading.
3. What should be the range of temperature for this experiment?
4. What should be the interval at which you need to take the reading?

3. Analysis

1. What graphs do you need to plot?
2. In Hall measurement experiment: report resistivity, carrier type and concentration, and mobility
3. In Four-point probe measurement: report room temperature resistivity and band gap
4. Compare room temperature resistivity of the two samples and comment.

4. Questions:

1. What is Hall Effect?
2. What are n-type and p-type semiconductors?
3. What is the effect of temperature on Hall coefficient of a lightly doped semiconductor?
4. Does the hole actually move?
5. Why resistances of the sample increase with increase of magnetic field?
6. What is advantage of four probe method over the conventional methods?

Appendix A

Correction factor for Four-point-probe measurement

For arbitrary shaped samples of finite geometry, the resistivity is given by

$$\rho = 2\pi dF(V/I) \quad (1)$$

where, F is the correction factor which corrects for probe location near sample edges, for sample thickness, sample diameter, probe placement, and sample temperature. It is usually a product of several independent correction factors. For samples thicker than the probe spacing, the simple, independent correction factors contained in F of above eqn. are no longer adequate due to interactions between thickness and edge effects. Fortunately, the samples are generally thinner than the probe spacings, and the correction factors can be independently calculated. For *collinear* or *in-line probes* with equal probe spacing, d, we write F as a product of three separate correction factors

$$F = F_1 F_2 F_3$$

Each of these factors can be further subdivided. F_1 corrects for sample thickness, F_2 for lateral sample dimensions, and F_3 for placement of the probes relative to the sample edges. Most four-point probe measurements are made with insulating bottom boundaries.

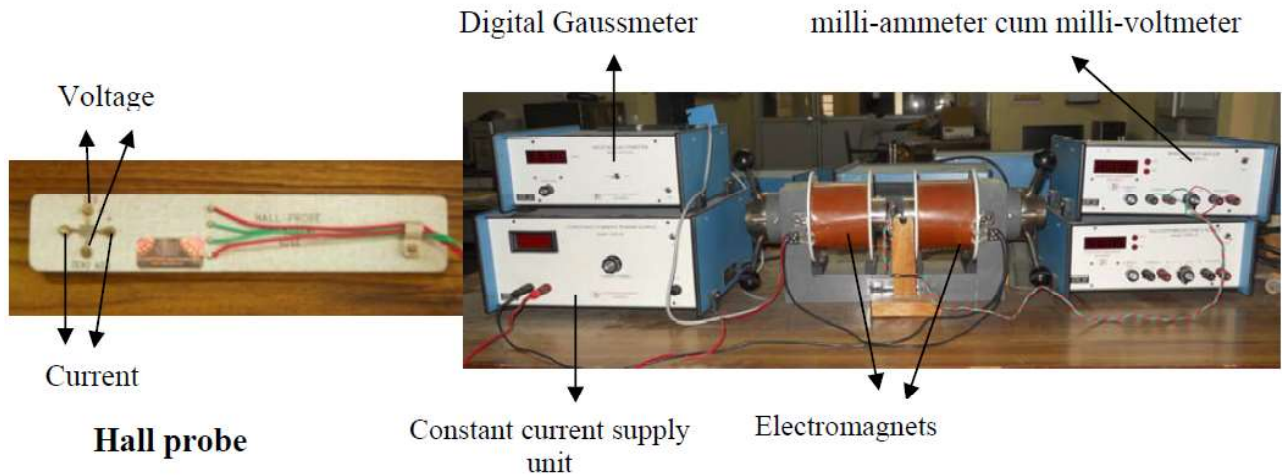
For very thin samples, i.e. $t \leq d/2$, $F_1 = (t/d)/2 \ln 2$, where t is sample thickness and F_2 and F_3 are approximately equal to unity. Therefore eqn (1) becomes

$$\rho = 4.532 t \frac{V}{I} \quad (2)$$

where, t is in cm, V is in volts and I is in amperes. (The value of ρ would be in ohm.cm)

Appendix B

1. Hall measurement set-up:



The Hall effect measurement set up is shown below with labeled important parts. The specifications of the instrument are:

1. Hall probe:
 - a. Contacts : Spring type (solid silver)
 - b. Hall voltage: 0.1-1 volt
 - c. Thickness of Ge crystal: 0.4
 - d. Resistivity: $10 \Omega \text{ cm}$
2. Digital milli-voltmeter:
 - a. Range: 0-200mV
 - b. Resolution: $100\mu\text{V}$
 - c. Accuracy: 0.1% of reading 1 digit
3. Constant current power Supply:
 - a. Current range: 0-4 A
 - b. Resolution: $10\mu\text{A}$
 - c. Load Regulation: 0.1%
 - d. Line Regulation: 0.1%
4. Electromagnet, EMU-50V:
 - a. Field intensity: 7.5 Gauss at 10mm Gap
 - b. Pole pieces: 50 diameters
 - c. Yoke material: U shaped soft iron
 - d. Power Requirement: 0-30V@4.0A

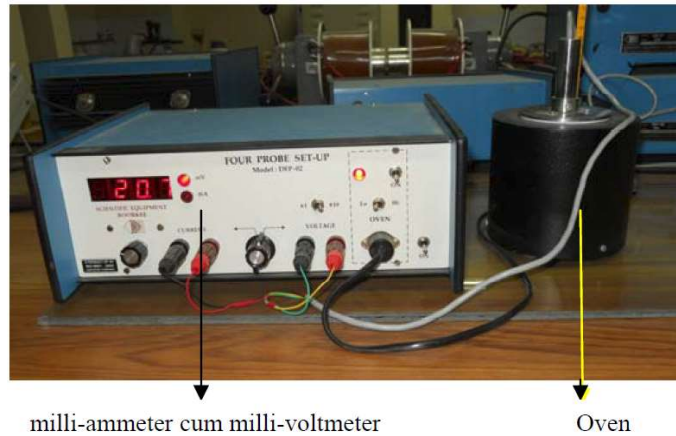
Procedure:

1. Calibrate the Gaussmeter by adjusting the current in the constant current supply unit and note down the value of magnetic field corresponding to it.
2. Connect the widthwise contacts of the Hall Probe to the terminals marked Voltage and lengthwise contacts to terminals marked Current.
3. Switch ON the Hall Effect set up and set the current to an appropriate value (say 5 mA).
4. Switch over the display to voltage side. There may be some voltage reading even outside the magnetic field. This is due to imperfect alignment of the four contacts of the Hall Probe and is generally known as the Zero field potential. In all cases this error should be subtracted from the Hall voltage reading.
5. Now place the probe in the magnetic field and switch on the electromagnet power supply and adjust the current to any value. Rotate the Hall probe till it become perpendicular to magnetic field. Hall voltage will be maximum in this adjustment.
6. Now keeping the current constant, measure hall voltage as a function of magnetic field.
7. Keeping the magnetic field constant, vary the current and measure the hall voltage.

Precautions:

1. For Hall Effect set up, probe should be in middle of electromagnet before taking readings.
2. Before taking reading, zero adjustment is to be done.

2. Four probe set up



A four probe set up is shown above with following specifications:

1. Oven: Temperatures can go up to 200°C
2. Current: 0-200 mA
3. Voltage: 0-200 mV

Procedure:

1. Fix the current to say 5mA.
2. Increase the temperature and measure the corresponding values of voltage at appropriate intervals.
3. The band gap energy can be calculated using the standard relation.

Precautions:

1. For band gap measurement, current is fixed at 5 mA , so do not change it.
2. Do not take specimen out from the furnace, when it is hot.

Experiment 11

(a) Microstructure of Metals and Alloys

(b) Quantitative Metallography

Theory:

When two or more elements combine in such a way that the elements are mixed on a atomic scale, the product is called an alloy or solid solution. Generally a solid solution is consists of single phase. The element with highest quantity in the solution is called the solvent and the rest elements are known as solutes. Unlike pure metals, alloys generally freeze over a range of temperature. During solidification of an alloy, this feature introduces compositional in homogeneity, which is reflected in the microstructure.

Columnar Grains : Macrostructure of Pure Zn

When a melt is poured into a container which is at a much lower temperature than the melt, large undercooling occurs in the regions where the melt comes into contact with the container walls. The liquid is cooled below its freezing temperature and the nucleation of the solid phase occurs adjacent to the walls. The formation of these solid crystals releases the latent heat of fusion and the degree of supercooling is reduced in liquid adjacent to these crystals. Consequently no fresh nuclei form in the center of the mold and the growth of the crystals formed near the mold wall continue inwards. The direction of growth of the crystals is opposite to the direction of the heat flow from the center of the ingot to the container walls. This results in long columnar crystals perpendicular to the walls. Sidewise growth is inhibited by neighboring grains, so the growing grains become *columnar* in shape. Fig 8.10. The grains in the columnar zone have different orientations from each other because they are differently oriented in the plane normal to the heat direction. Later, grains may begin to form within the interior of the melt, and grow approximately equally in all directions. Such grains are called *equiaxed*.

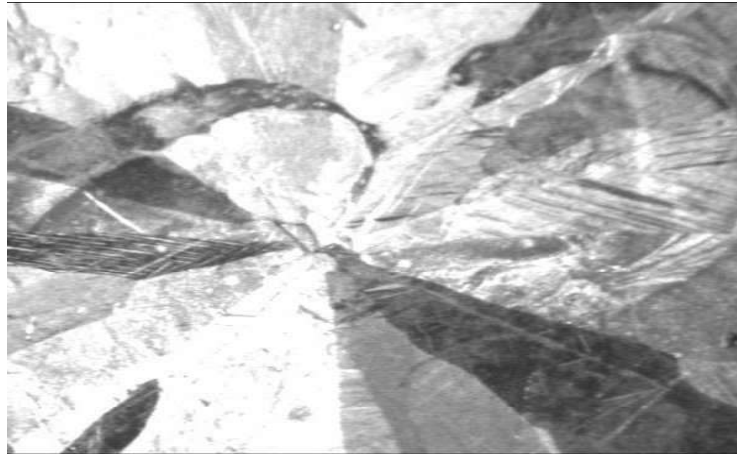


Fig 8.10 Long Columnar grains of Pure Zinc

Dendritic Growth: Microstructure of Cu-Ni

The initial stage of solidification of an alloy is similar to that for a pure metal. During the period of columnar growth, however, the solid phase develops protuberances. This is because the solute atoms are rejected during the formation of the solid phase and the liquid in the immediate vicinity of the solid- liquid interface is enriched with solute. This liquid has a lower freezing temperature. Since the interface can be assumed to be at equilibrium and the actual temperature gradients quite small, the liquid ahead of the interface is supercooled and the supercooling increases with the distance from the interface. As a result, any solid protuberance ahead of the plane interface grows more rapidly than the plane interface since the liquid solidifies more readily with increased supercooling. The resulting branched crystal often has the appearance of a miniature pine tree and is accordingly called a *dendrite* after the Greek word dendrites meaning “of a tree”. The direction in which these spikes grow is crystallographic and is known as the dendritic growth direction. The direction of dendritic growth depends on the crystal structure of a metal. (Fig8.1). The phase diagram of Cu-Ni is shown in Fig.8.2.

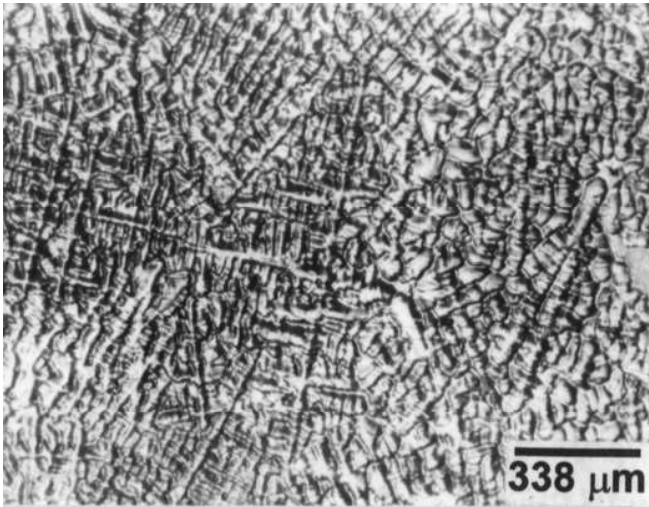


Fig.8.1 Dendritic microstructure

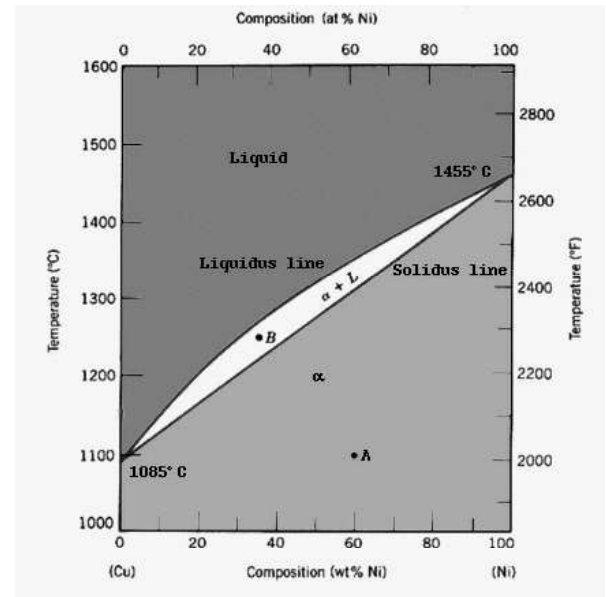


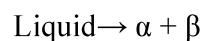
Fig.8.2 Cu - Ni Phase diagram

The region above liquidus line is liquid and below solidus line is solid and the intermediate region is called the mushy zone where liquid and solid co-exist. From phase diagram it is obvious that as the composition of solute nickel increases the freezing temperature is increasing and at temperature higher than 1455 °C (M.P. of Ni) it is totally liquid for any composition of nickel. At temperature below 1085 °C (M.P. Cu) the alloy is totally solid and only a single phase is obtained at room temperature for any composition of nickel in copper. Copper and nickel form in the solid state a continuous series of fcc mixing crystals. The strength of copper-nickel alloys rises with the Ni content; at about 60% Ni the maximal value is obtained at a still good toughness; the breaking stress there is more than 40%. Much used Cu-Ni alloys are: Cupronickel, Cu with 10-30% Ni and about 1%Fe.

Two phase structure:

(i)Eutectic structure: Microstructure of Cu-P

In eutectic structure reaction a liquid phase transforms into a mixture of two solid phases with different compositions and crystal structures.



on cooling, the melt with composition C in Fig 8.5 forms a two phase microstructure with crystals of α and β . The initial formation of a α crystal causes the surrounding liquid to be super saturated in β with the result that the condition are favourable form the nucleation

and growth of a β crystal next to the α crystal already formed. The Microstructure of Cu/8.4 wt % P alloy shows the grains composed of colonies of fine eutectic structure A lamellar pattern consisting of crystals of copper rich solid solution (dark) and copper phosphide (Cu_3P) (white) is observed.(Fig. 8.4)

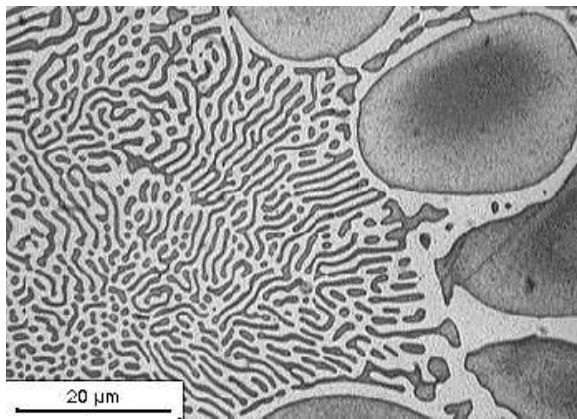


Fig 8.4 Microstructure of Cu-4.5wt%P

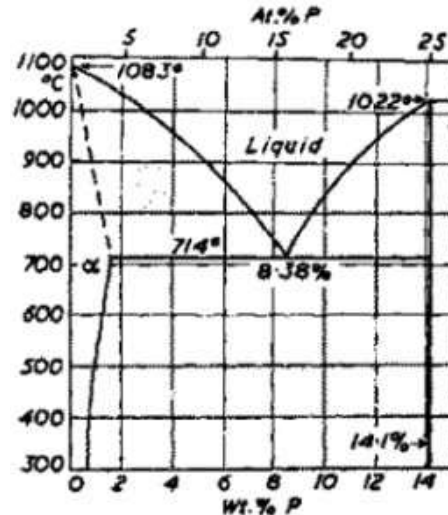
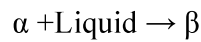


Fig 8.5 Cu-P Phase diagram

(ii) Peritectic Structure: Microstructure of Cu-Zn

In peritectic reaction a solid and a liquid phase react to produce another solid phase.



If the melt composition C in is cooled below temperature T_p , the product phase β starts to form at the interface between α and liquid. The growth of this phase is dependent on the diffusion of atoms on one side of β to the other side. Since diffusion is slow in solid state, equilibrium microstructures are rarely obtained in peritectic systems. The microstructure shows crystals of copper rich solid solution (light etching), partly surrounded by β crystals (dark) are observed. β crystals have formed by peritectic reaction Fig 8.6. The phase diagram of Cu-Zn is shown in Fig.8.7.



Fig 8.6 Microstructure of Cu-Zn
Polycrystalline Structure: Microstructure of Cu

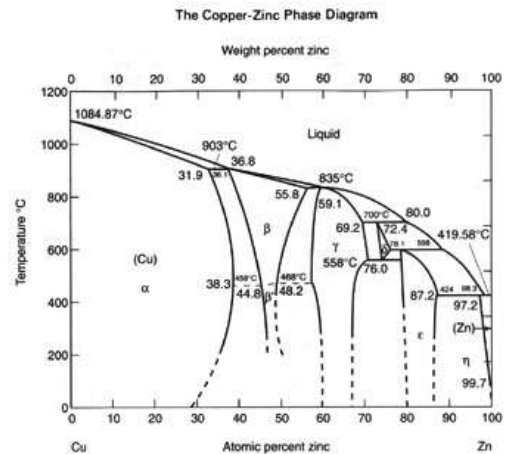


Fig 8.7 Phase diagram of Cu-Zn

Most metals are commonly found in polycrystalline form. That is, the material is composed of many small regions, called grains that have different orientations of the crystal structure. Between the grains are grain boundaries, which are regions of extreme disorder in the crystal structure. Due to this disorder acids and other etchants typically attack (react with) the grain boundary material first. This provides a method for making the grain boundaries visible in an optical microscope. The image below (Fig 8.8) shows some typical grains in the polycrystalline copper discussed here. The strength of a polycrystalline metal increase as the grain size decreases; this is known as the Hall-Petch effect, after the scientists who first studied it.

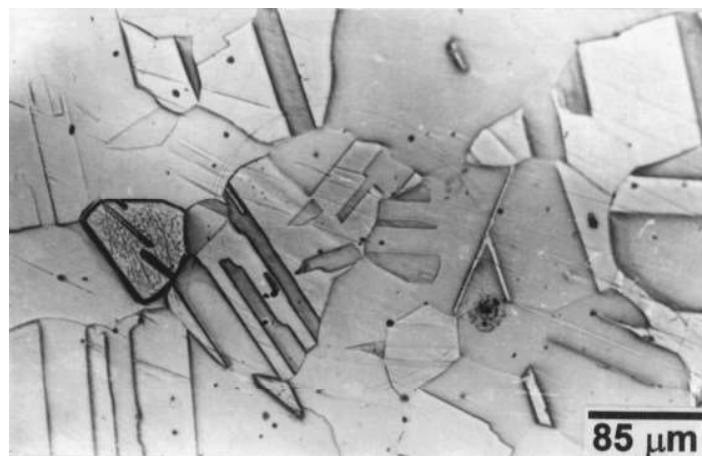


Fig 8.8 Microstructure of Copper

(b)Quantitative Metallography : Measuring Volume Fraction

Volume Fraction, Areal Analysis

1. Trace the structure onto paper, weight the paper, cut out the parts containing the phase of interest and weigh these parts. The weight fraction equals the area fraction of phase in this section. The average of a number of area fraction measurements gives one the volume fraction of phase.

2. Etch the specimen to color each phase differently. Use a computer to measure the area of each phase (color). The average of number area fraction measurements is equal to the volume fractions of phases.

Volume Fraction, Lineal Analysis

Using lines uniformly distributed but randomly oriented, the average length of the line segments crossing the selected phase is equal to the area fraction of the phase viewed in the planar section. The average of number area fraction measurements is equal to the volume fractions of phases.

Volume Fraction, Point Count

The fraction of a number of points which fall on the selected phase is equal to the area fraction of that phase. The average of a number of area fraction measurements is equal to the volume fractions of phases.

Recommended Method

Measurement of Volume Fraction of Phases Using the Systematic Point Count Method

This method (Fig 8.9) is based on the fact that the average fraction of points which fall on grains of a particular phase is equal to the area fraction of the phase in the polished section and that the average of these area fractions is equal to the volume fraction of the phase.

This method entails selecting a suitable array of points, overlaying it on the specimen and counting the points which fall on the selected phase, selecting a new are and counting again, and again until the desired error is obtained. The procedure is as follows:

1. The most efficient method will be that which requires the least effort per observation.
2. Using a reticule grid and observing the polished sample is more efficient than using a micrograph.

3. A square array of points is simple, symmetric and easy to obtain.
4. The optimum number of points in the grid large to minimize the effort of changing views (or micrographs) and minimum to reduce the effort of counting. .
5. Select an area on the specimen where counts are to be made. This selection should be made at random or per a predefined pattern so as to minimize bias.
6. Count each point which falls on the selected phase.
10. Assign a count value of $\frac{1}{2}$ to points which fall on inter phase boundaries.
11. Tabulate the Results
12. Compute the mean
13. Divide these by the number of points in the grid and multiply them by 100. This gives the results in terms of the volume percent of phase.

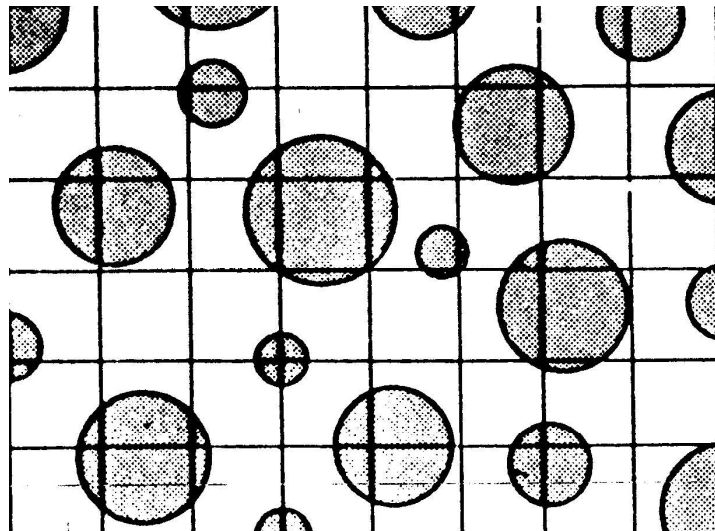


Fig 8.9. Point count method

EXPERIMENT 12

MAGNETIC HYSTERESIS OF NICKEL

Aim:

To study the magnetization behaviour with alternating magnetic field and report (i) hysteresis curve (ii) H_c (iii) B_s (iv) B_r

Theory:

Magnetic Materials

All magnetic materials exhibit spontaneous magnetic moment - a magnetic moment even in zero magnetic field. They have ordered arrays of magnetic moments, i.e. electron spins and spin magnetic moments are arranged in a regular manner, as illustrated

in Fig. 6.1. Magnetic materials can be classified into ferromagnetic [spins aligned in the same direction or parallel, equal moments of one type only, e.g. Fe, Co, Ni, Gd], antiferromagnetic [spins on neighboring atoms in opposite directions or antiparallel, all moments of one type only and equal, net saturation magnetic moment nil, e.g. Cr], and ferrimagnetic [spins on neighboring atoms in opposite directions or antiparallel, but more than one type of moment present with unequal moments, e.g. $\text{NiO} \cdot \text{Fe}_2\text{O}_3$, occurs in compounds only], See Fig. 6.1

Ferromagnetic Domains

In a ferromagnetic specimen, often, the net magnetic moment is much less than what one would expect from the sum of magnetic moments of all the individual atoms, and application of an external magnetic field is required to obtain the saturation magnetic moment. This phenomenon is explained by the presence of magnetic domains. A domain is a small region in a magnetic material, within which the local magnetization is saturated, i.e. spins on all the atoms are parallel.

However, the directions of magnetization of different domains do not coincide, as illustrated in Fig. 6.2, resulting in a small resultant magnetic moment. Magnetic domains are responsible for the hysteresis loop. Fig. 6.3 represents the magnetization curve, i.e. magnetization M as a function of the external magnetic field H , of a ferromagnetic material. It is assumed that the net magnetization was zero for the specimen, before the application of the external magnetic field. The increase in the magnet moment of the specimen under the action of an applied magnetic field takes place by two independent

processes: [i] in weak applied fields, the volume of domains which are favorably oriented with respect to the field increases at the expense of unfavorably oriented domains, See Fig. 6.3 [ii] in strong applied fields, the magnetization rotates toward the direction of the field. These two processes can explain why a loop is traced in the B-H plane, as the magnetic field completes a cycle. Technical terms defined by the hysteresis loop are shown in Fig.6 3.

The domain structure of ferromagnetic materials affects their practical properties. In a transformer core, we want a high permeability $\mu = B/H$. In a permanent magnet, we want a high coercive force. By suppressing the possibility of boundary displacement, we may achieve a high coercivity, the suppression may be accomplished by using very fine particles or by precipitating a second metallurgical phase, so that the specimen is heterogeneous on a very fine scale. By making the material pure homogeneous and well oriented we facilitate domain boundary displacement, and thereby attain high permeability.

The area of the hysteresis loop represents an energy loss. In industrial applications, magnetic materials are classified on the basis of the loop area and characteristics. Soft magnetic materials have low hysteresis and eddy current losses, and high magnetic permeability. [Eddy currents flow in a magnetic material due to the induced emf. This current has a corresponding I^2R loss.] These materials [e.g. 97Fe3Si, Fe₂O₃, NiO.Fe₂O₃] industrially are most important.

Hard magnetic materials [e.g. Alnico 5: 51Fe14Ni24Co8Al3Cu], on the other hand, have high coercivity, and large remanent and saturation magnetizations.

Hence, to characterize any magnetic material, it is necessary to obtain its hysteresis loop.

Measurement Setup:

The hysteresis loop measurement setup has three components: [i] the solenoid-specimen-pickup coil combination; [ii] the loop tracer control cabinet; and [iii] the oscilloscope for loop tracing.

The magnetic specimen is a Ni wire, 1.13 mm in diameter, 44 mm in length. To obtain its hysteresis loop, the ac hysteresis loop tracer will be used. The magnetic field is provided by a solenoid, into which the magnetic specimen is placed. A pick-up coil is used to monitor the magnetization of the specimen. The specimen, the pick-up coil, and

the solenoid are, coaxial. The pick-up coil is shorter than the specimen in length, is located in the center of the specimen, and closely encircles the specimen.

The hysteresis loop tracer feeds to the x-axis of an oscilloscope a signal proportional to the magnetic field H , and to the y-axis a signal proportional to the magnetization M . Hence, as the applied magnetic field is sinusoidal, a loop is traced on the oscilloscope, for a given magnitude of the applied sinusoidal magnetic field. This loop will not only increase in size with the magnitude of the sinusoidal field, but will also change in shape. For low to medium magnitudes, the loop shape will be rectangular to parallelogram. At high magnitudes, it will approach the form of Fig. 6.3, and will indicate saturation of magnetization.

Several problems are encountered in practice while measuring the hysteresis loop. The magnetic field becomes non-uniform on account of: [i] open specimen; and [ii] fields induced by the eddy current. The eddy currents also cause the forward and backward paths traced near saturation magnetization to be different, thereby leading to a small loop inside the large loop in the saturation region.

Experimental Procedure:

1. Inspect the measurement setup, in particular the solenoid-specimen-pickup-coil combination and the loop tracer control panel.
2. Calibration of the oscilloscope and settings of the area ratio and demagnetization factor.
3. Record: [i] loop shape; [ii] loop width [in mm]; [iii] tip to tip height [in mV]; and [iv] y-axis intercept, [in mV] for magnetic fields of 50, 100, 150, 200, 250, and 300 Gauss.
4. The loop shape is to be recorded as free-hand sketches on the result sheet. The values of field, loop width, tip to tip height, and y-axis intercept are to be put in a tabular form.
5. From the table, estimate the saturation magnetization M_s in mV [= half the asymptotic value of the tip to tip height], the remanent magnetization M_r in mV [= the asymptotic value of the y-axis intercept]. To estimate the coercivity H_C in mm, plot on a small-size graph paper the loop width versus the field. Take H_C as half the value of the intercept of the linear part of the plot for zero field.

6. Calculate H_C in Oersted, M_r in Gauss, M_S in Gauss, using the following relations:

$$1 \text{ mm} = 8.58 \text{ Oe}$$

$$1 \text{ mV} = 2.63 \text{ G}$$

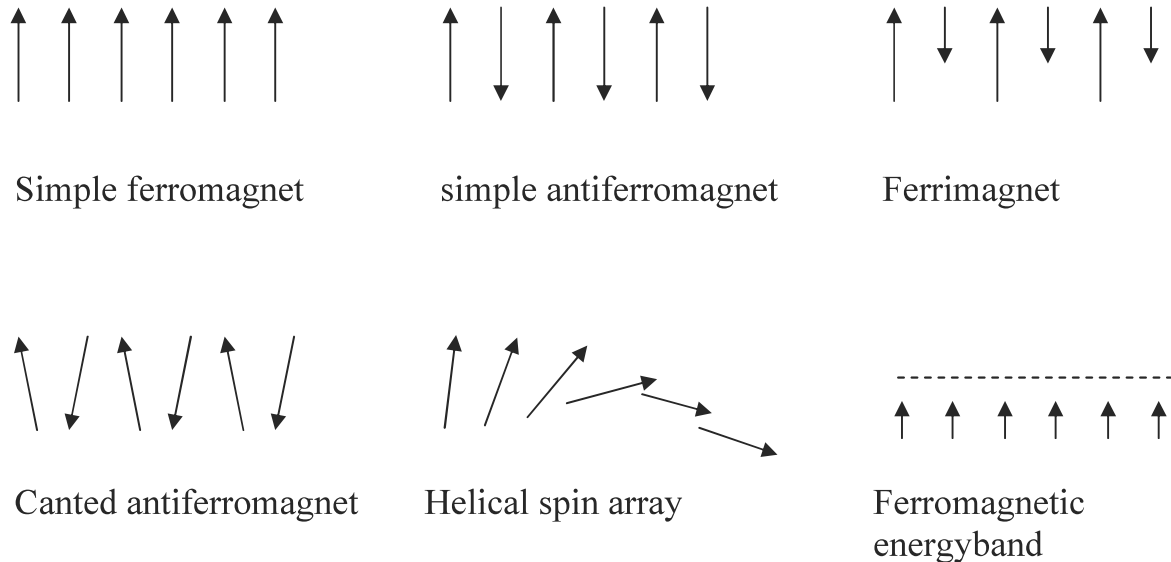


Fig 6.1 Possible ordered arrangements of electron spins.

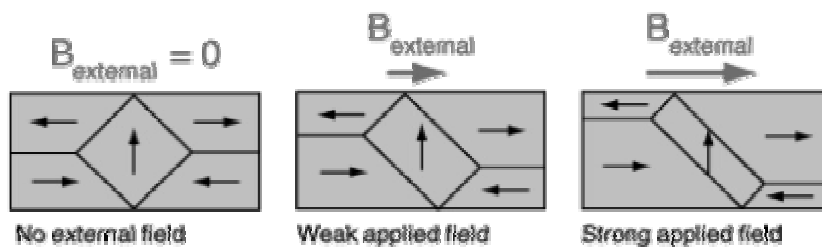


Fig 6.2 Magnetic domains behavior with applied field

These illustrations of domains are conceptual only and not meant to give an accurate scale of the size or shape of domains. The microscopic evidence about magnetization indicates that the net magnetization of ferromagnetic materials in response to an external magnetic field may actually occur more by the growth of the domains parallel to the applied field at the expense of other domains rather than the reorientation of the domains themselves as implied in the sketch

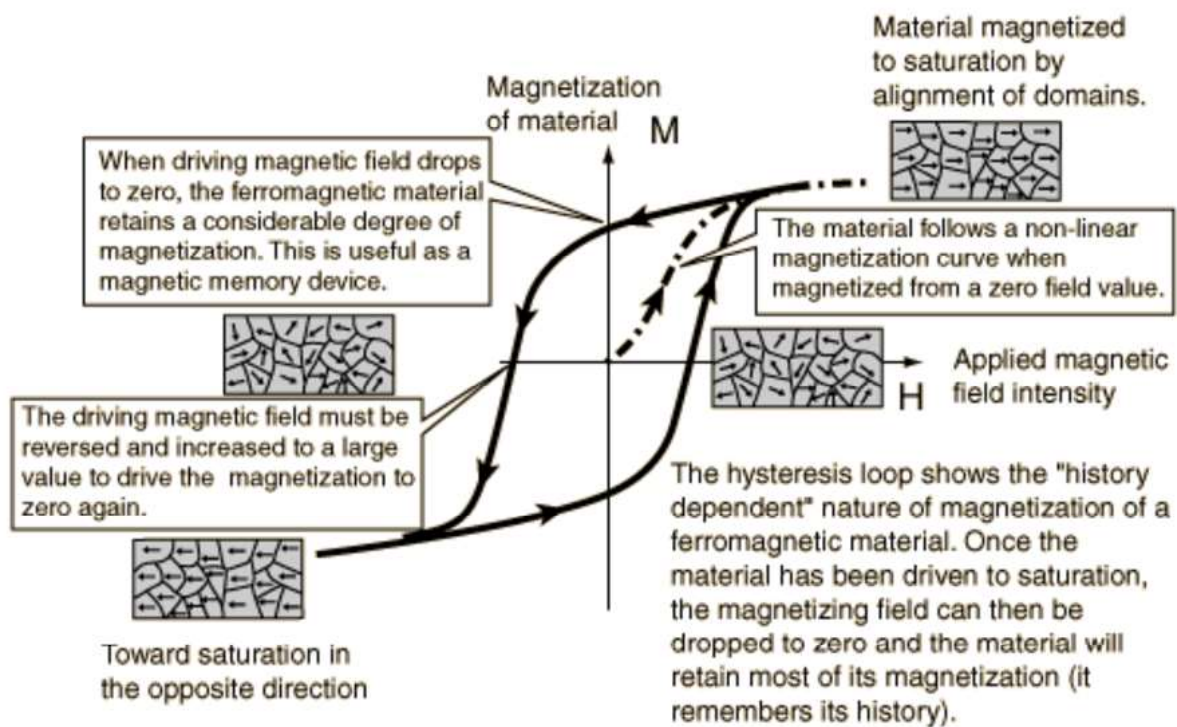


Fig 6.3a Magnetisation Curve

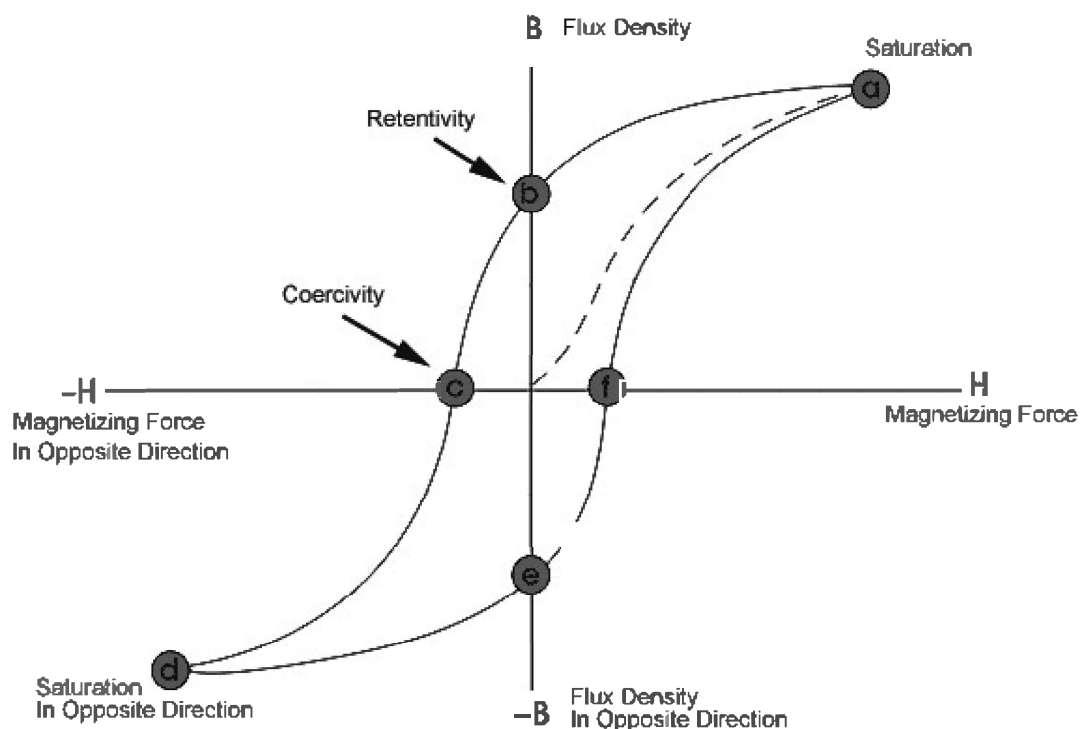


Fig 6.3b Magnetisation Curve

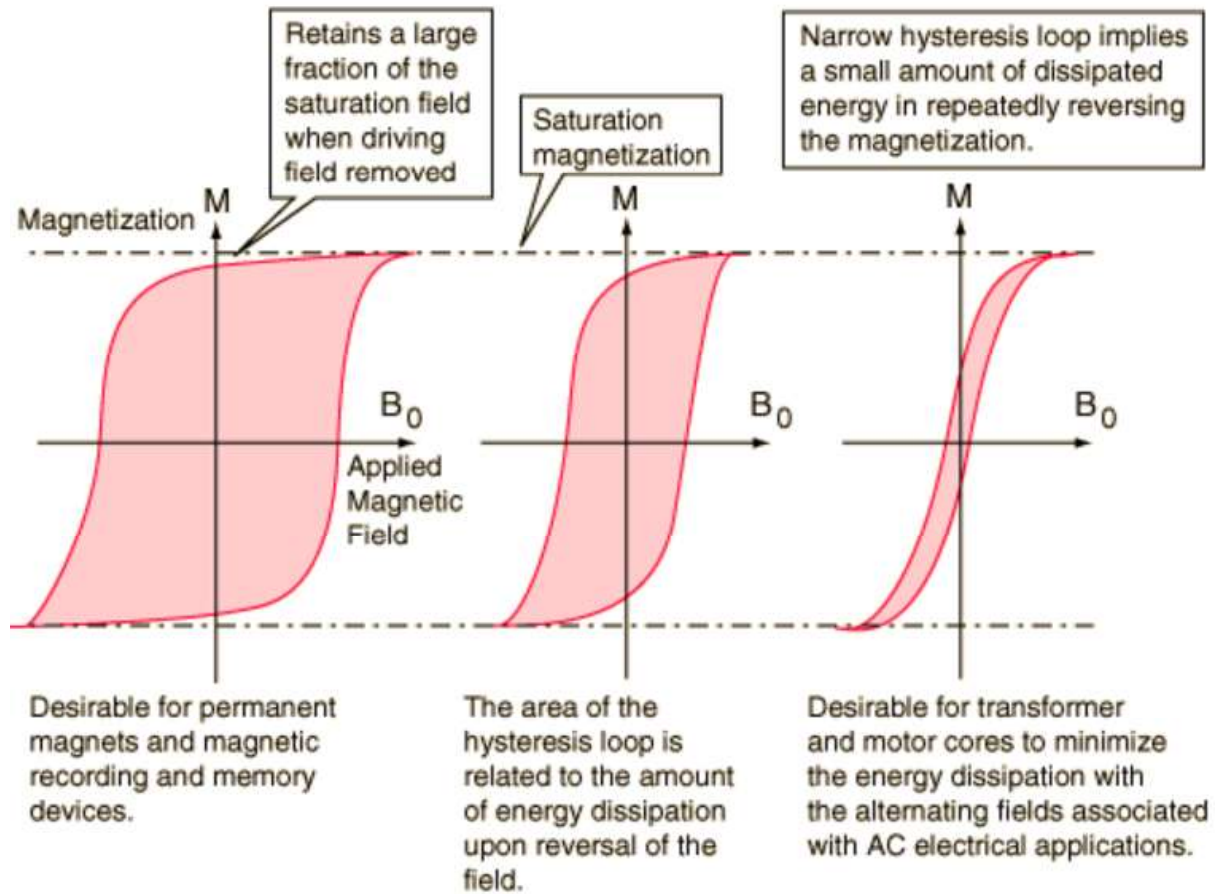


Fig 6.3c Magnetisation Curve

Questions:

1. Why there is an extra secondary loop appears top and bottom of the hysteresis loop along with the original loop?
2. Explain the difference in B-H Loop of hard and soft iron samples?